



Shallow Depth, Substantial Change: Fluid-Metasomatism Causes Major Compositional Modifications of Subducted Volcanics (Mariana Forearc)

Elmar Albers^{1*}, John W. Shervais², Christian T. Hansen¹, Yuji Ichiyama³ and Patricia Fryer⁴

¹MARUM – Center for Marine Environmental Sciences, University of Bremen, Bremen, Germany, ²Department of Geology, Utah State University, Logan, UT, United States, ³Graduate School of Science, Chiba University, Chiba, Japan, ⁴School of Ocean and Earth Science and Technology, University of Hawaii at Manoa, Honolulu, HI, United States

OPEN ACCESS

Edited by:

Philipp A. Brandl,
Helmholtz Association of German
Research Centres (HZ), Germany

Reviewed by:

Xu Chu,
University of Toronto, Canada
Jeffrey Alt,
University of Michigan, United States

*Correspondence:

Elmar Albers
e.albers@uni-bremen.de

Specialty section:

This article was submitted to
Petrology,
a section of the journal
Frontiers in Earth Science

Received: 30 November 2021

Accepted: 23 February 2022

Published: 01 April 2022

Citation:

Albers E, Shervais JW, Hansen CT,
Ichiyama Y and Fryer P (2022) Shallow
Depth, Substantial Change: Fluid-
Metasomatism Causes Major
Compositional Modifications of
Subducted Volcanics
(Mariana Forearc).
Front. Earth Sci. 10:826312.
doi: 10.3389/feart.2022.826312

Mass transfer at shallow subduction levels and its ramifications for deeper processes remain incompletely constrained. New insights are provided by ocean island basalt (OIB) clasts from the Mariana forearc that experienced subduction to up to ~25–30 km depth and up to blueschist-facies metamorphism; thereafter, the clasts were recycled to the forearc seafloor *via* serpentinite mud volcanism. We demonstrate that the rocks were, in addition, strongly metasomatized: they exhibit K₂O contents (median = 4.6 wt%) and loss on ignition (median = 5.3 wt%, as a proxy for H₂O) much higher than OIB situated on the Pacific Plate, implying that these were added during subduction. This interpretation is consistent with abundant phengite in the samples. Mass balance calculations further reveal variable gains in SiO₂ for all samples, and increased MgO and Na₂O at one but losses of MgO and Fe₂O₃* at the other study site. Elevated Cs and Rb concentrations suggest an uptake whereas low Ba and Sr contents indicate the removal of trace elements throughout all clasts. The metasomatism was likely induced by the OIBs' interaction with K-rich fluids in the subduction channel. Our thermodynamic models imply that such fluids are released from subducted sediments and altered igneous crust at 5 kbar and even below 200°C. Equilibrium assemblage diagrams show that the stability field of phengite significantly increases with the metasomatism and that, relative to not-metasomatized OIB, up to four times as much phengite may form in the metasomatized rocks. Phengite in turn is considered as an important carrier for K₂O, H₂O, and fluid-mobile elements to sub-arc depths. These findings demonstrate that mass transfer from the subducting lithosphere starts at low *P/T* conditions. The liberation of solute-rich fluids can evoke far-reaching compositional and mineralogical changes in rocks that interact with these fluids. Processes at shallow depths (<30 km) thereby contribute to controlling *which components* as well as *in which state* (i.e., bound in which minerals) these components ultimately reach greater depths where they may or may not contribute to arc magmatism. For a holistic understanding of deep geochemical cycling, metasomatism and rock transformation need to be acknowledged from shallow depths on.

Keywords: fluid metasomatism, seamount subduction, Mariana subduction zone, forearc devolatilization, blueschist metamorphism, geochemical cycling, phengite, International Ocean Discovery Program (IODP)

INTRODUCTION

Geologic processes in subduction zones are among the main controllers of chemical cycling (e.g., Stern, 2002, and references therein) that had and still have severe implications for the geochemical evolution and differentiation of Earth. Most importantly, such processes include the liberation of fluids from the subducting slab at ~70–120 km depths that then migrate into the overriding plate where they provoke hydrous partial melting of the mantle. This in turn results in magmatism, tholeiitic to calc-alkaline volcanism, and, over long periods of time, the formation of island arcs and continental crust (e.g., Ringwood, 1969; Peacock, 1990; Taylor and McLennan, 1995).

In greater detail, it is the breakdown of hydrous minerals contained in subducting sediments and hydrothermally altered igneous crust and mantle that causes the release of H₂O during prograde subduction metamorphism (e.g., Poli and Schmidt, 1995). Together with the fluids, which act as primary transport agents for mass in subduction systems, elements are mobilized and transported into the subduction channel (i.e., the zone at the slab–wedge interface containing the subduction mélange) and the mantle wedge (e.g., Bebout et al., 1999; Scambelluri and Philippot, 2001; Ulmer, 2001). Consequently, arc eruptives commonly exhibit a trace element signal indicative of sources that include metasomatized slab-derived components (e.g., Manning, 2004; Rustioni et al., 2021). Eruptives are for instance typically enriched in the incompatible elements B, K, Sr, Cs, Ba, U, and Pb that are traditionally interpreted to originate from sediments and altered oceanic basement and are known as the “slab signature” (Perfit et al., 1980; Tatsumi and Eggins, 1995; Codillo et al., 2018). Arc eruptives provide an important window into deep subduction processes and elemental cycling, which have been in the focus of petrologic/geochemical, experimental, and modeling studies over several decades.

Much dehydration of the subducted lithologies, however, occurs long before these reach sub-arc depths. Subducting altered and hydrated basalts, for example, may contain up to 5 wt% H₂O—the bulk of which is released during the breakdown of hydrous phases as subduction metamorphism causes the transformation to blueschist (~3 wt% H₂O) and amphibolite (~1–2 wt% H₂O) facies assemblages (Poli and Schmidt, 1995). H₂O release from underthrust sediments, due to the compaction and release of interstitial pore waters and mineral dehydration, start as soon as they are subducted (e.g., Moore and Vrolijk, 1992; Bekins et al., 1994). This liberation of fluids at shallow depths is likewise accompanied by significant mass transfer. Slab-derived fluids from several subduction zones have been shown to carry high loads of solutes, in particular elements that are “fluid-mobile” (e.g., at the Nankai Trough or Costa Rica; see review by Kastner et al., 2014).

Whereas slab-derived fluids could be studied at several active convergent margins, most rocks that experienced (and recorded) interactions with such fluids at low- to intermediate-depth subduction conditions originate from paleo-subduction settings. Based on these rocks, now exposed on land, a number of studies advocate minimal fluid and element mobility at low metamorphic grades (e.g., Busigny et al., 2003;

Ghatak et al., 2012; see also review by G. E. Bebout in Harlov and Austrheim, 2013). The only active system that provides direct insight into depths of up to blueschist-facies conditions is the Mariana convergent margin. Here, recent ocean research drilling efforts (Fryer et al., 2018) have recovered rocks that differ in composition from what has initially been subducted. In this communication we demonstrate that these rock samples are strongly metasomatized and that the changes in composition can well be explained by their interaction with slab-derived fluids. Our study highlights that the metasomatism to a large degree affects mineralogical assemblages of the lithologies involved, which in turn will affect deeper processes such as the composition of arc magmas and geochemical cycling.

Serpentinite Mud Volcanism at the Mariana Forearc

The Mariana Trench in the northwestern Pacific marks the subduction of the >180 My old Pacific Plate beneath the Mariana forearc. Together with altered igneous crust, a ~460 m thick sedimentary cover composed of siliceous ooze, volcanoclastic deposits, and pelagic clays is being subducted (Plank et al., 2000; Leat and Larter, 2003). Compaction and early, low-temperature mineral dehydration result in the release of fluids from the incoming lithologies soon after their subduction; these fluids, in turn, hydrate and serpentinize the overlying Mariana forearc mantle wedge (e.g., review by Fryer, 2012). The serpentinite is partly comminuted by tectonic movements and shearing processes at the slab–wedge interface, and deep faults within the forearc crust and mantle facilitate the buoyancy-driven rise of the serpentinite and slab-derived fluids to the forearc seafloor where these erupt in episodic mudflows. Over millions of years, the mudflows have built vast mud volcanoes up to ~50 km in diameter and ~2 km high (Fryer et al., 1985; Fryer et al., 1992). More than a dozen of such serpentinite mud volcanoes are distributed over the forearc seafloor. They formed at varying distances to the Mariana Trench, tapping the subduction channel at subduction depths of ~13–30 km and temperature (*T*) of <80–350°C (Figure 1; e.g., Fryer et al., 1992; Oakley et al., 2008; Hulme et al., 2010). The serpentinite mud volcanism provides unparalleled insight into the shallow levels of an active subduction zone.

Five serpentinite mud volcanoes were sampled during three scientific ocean drilling campaigns: Yinazao (55 km distance to the Mariana Trench, ~13 km depth to the slab, ~80°C at the slab–mantle wedge interface), Fantangisña (62 km to trench, ~14 km to slab, ~150°C), and Asüt Tesoru (72 km to trench, ~18 km to slab, ~250°C) during International Ocean Discovery Program (IODP) Expedition 366 (Fryer et al., 2018), and South Chamorro and Conical (78 and 86 km to trench, 18 and 19 km to slab, respectively, with *T* = 250–350°C at the slab) during previous Ocean Drilling Program (ODP) legs (e.g., Fryer et al., 1992).

Beside serpentinite mud, recovered drill cores contain up to meter-sized boulders of the serpentinized mantle wedge but also materials that originate from the forearc crust and from the subducting Pacific Plate (see next section).

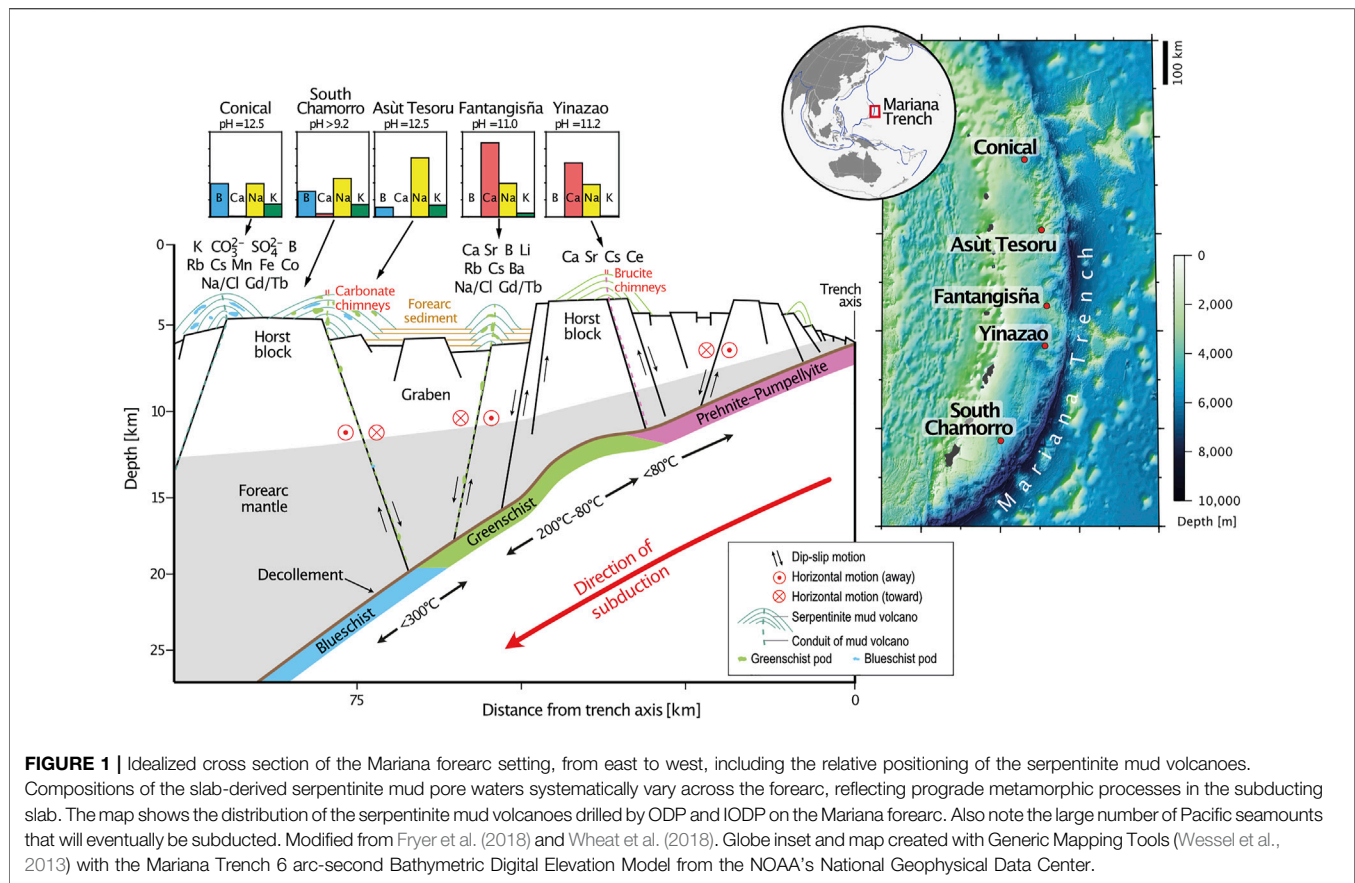


FIGURE 1 | Idealized cross section of the Mariana forearc setting, from east to west, including the relative positioning of the serpentinite mud volcanoes.

Compositions of the slab-derived serpentinite mud pore waters systematically vary across the forearc, reflecting prograde metamorphic processes in the subducting slab. The map shows the distribution of the serpentinite mud volcanoes drilled by ODP and IODP on the Mariana forearc. Also note the large number of Pacific seamounts that will eventually be subducted. Modified from Fryer et al. (2018) and Wheat et al. (2018). Globe inset and map created with Generic Mapping Tools (Wessel et al., 2013) with the Mariana Trench 6 arc-second Bathymetric Digital Elevation Model from the NOAA's National Geophysical Data Center.

Similar mud flow deposits have been described worldwide from subaerially exposed forearc regions as old as 3.8 By (e.g., Lockwood, 1972; Fryer et al., 1995; Giaramita et al., 1998; Pons et al., 2011; Wakabayashi, 2012), implying that serpentinite mud volcanism in forearc environments occurred throughout the geologic past but requires specific, considerably deformed non-accretionary convergent margin settings.

Serpentinite Mud Volcanism Recycles Subducted Volcanics

Rock fragments and clasts with mid-ocean ridge basalt (MORB) and ocean island basalt (OIB) provenances were discovered in cores from the serpentinite mudflows of several mud volcanoes. The materials vary in size from millimeter to meter scale and have been identified as subducted, metamorphosed, and recycled materials from the incoming Pacific Plate. Metamorphic mineral assemblages attest up to blueschist facies peak metamorphic conditions (e.g., Maekawa et al., 1993; Fryer et al., 2006; Ichiyama et al., 2021). Numerous such metamafic rocks were recently retrieved from the Yinazao, Fantangisña, and Asùt Tesoru mud volcanoes (Fryer et al., 2018). In addition, similar clasts have previously been sampled from South Chamorro and Conical Seamounts (e.g., Fryer et al., 1992). These materials are, to our knowledge, the only blueschist-facies rocks that have been recovered from any active subduction zone.

Petrographic descriptions and (mineral) geochemical compositions of the recycled OIBs from Fantangisña and Asùt Tesoru have been reported by Albers et al. (2019), Fryer et al. (2018), Fryer et al. (2020), Deng et al. (2021), and Ichiyama et al. (2021). In many samples, aphyric to coarse grained igneous textures are preserved; aside from rare relict Ti-rich augite, plagioclase, and traces of olivine, apatite, biotite, and Fe-Ti oxides, the igneous mineral assemblages are largely metamorphosed. The clasts are now composed of low- to high-pressure and low- to moderate- T metamorphic minerals. These include Ca pyroxene, Na and Ca-Na amphibole, pumpellyite, and phengite at both seamounts, with prehnite, calcite, and zeolites (analcime, thomsonite, natrolite) exclusively reported from Fantangisña and lawsonite and Na pyroxene from Asùt Tesoru (Albers et al., 2019; Fryer et al., 2020; Ichiyama et al., 2021). Metamorphic vein precipitates that formed in apparent equilibrium with slab-derived fluids include pectolite and prehnite at Fantangisña and lawsonite and phengite at Asùt Tesoru; metamorphic calcite and aragonite occur at both sites (Albers et al., 2019). Na pyroxene mainly ranges in composition from aegirine to jadeite, but some analyses exhibit an increased augite component; amphibole is riebeckitic with ferric Fe/Al ratios of up to ~ 0.45 indicating a strong glaucophane component; phengite is Si-rich with up to 3.88 Si per formula unit (Albers et al., 2019; Fryer et al., 2020; Deng et al., 2021; Ichiyama et al., 2021). These phase assemblages and compositions

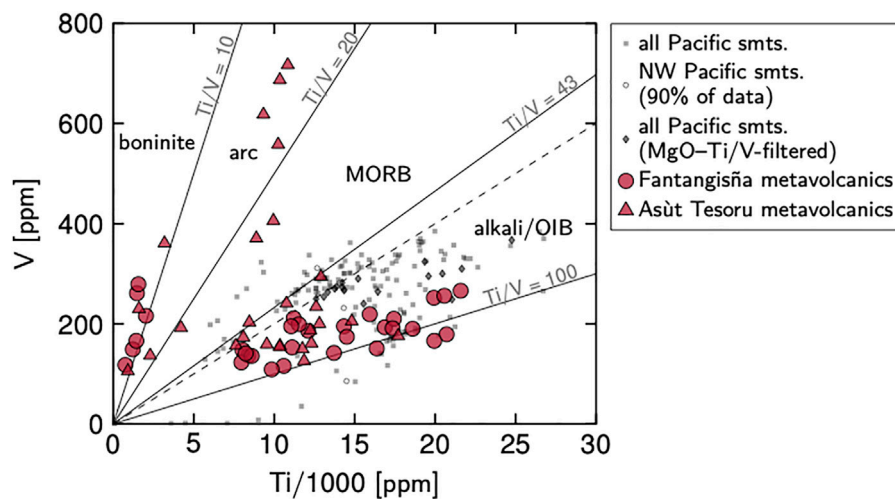


FIGURE 2 | Bulk rock Ti–V systematics of metamafic clasts recovered during IODP Exp. 366. An OIB provenance is implied by Ti/V ratios between 43 and 100 (Shervais, 2021; the dashed line marks the now revised discrimination line of Ti/V = 50 after Shervais, 1982) for the clasts from Fantangisña and Asüt Tesoru Seamounts that are discussed in this paper. Data from Fryer et al. (2020) and Deng et al. (2021). Compositions of Pacific seamounts are shown for comparison (see *Methods* for more information and data sources).

led Ichiyama et al. (2021) to suggest peak metamorphic grades of prehnite–pumpellyite facies for the clasts from Fantangisña Seamount and of blueschist facies for those from Asüt Tesoru.

The OIB origin of the clasts is implied by bulk rock Ti/V ratios between 50 and 100 (**Figure 2**; Fryer et al., 2020; Deng et al., 2021; note that the Ti–V discrimination diagram was recently revised by Shervais, 2021) and by the presence of titanium augite (e.g., Albers et al., 2019). Geochemically, concentrations of SiO₂, MgO, and Na₂O in the recycled OIBs appear to generally overlap with those of volcanic seamounts situated on the Pacific Plate but Fe₂O₃* (= FeO + Fe₂O₃) and CaO are generally lower whereas K₂O and loss on ignition (LOI) are much higher (**Figure 3** and **Table 1**; Fryer et al., 2018; Deng et al., 2021). These distinct compositions have, however, not received particular attention in the above studies. In this work, we will focus on the (modified) compositions of the recycled OIBs, which we attribute to fluid-metasomatism that occurred in the subduction zone, and its implications for mass transfer and geochemical cycling.

METHODS

Bulk Rock Geochemistry

To expand the existing dataset by Fryer et al. (2018) and Deng et al. (2021) we have analyzed four additional OIB samples for their major element bulk compositions. Analyses were carried out with a Panalytical® 2400 sequential X-ray fluorescence spectrometer at Utah State University using methods described in Shervais et al. (2019).

OIB Reference Compositions

As reference OIB compositions we downloaded data from the PetDB Database (www.earthchem.org/petdb) on 16–02–2021. We extracted all entries with the label “Seamount” situated in the

Pacific Ocean ($n = 3,216$). We then narrowed down the composition representative for alkali basalt/OIB by filtering 1) for Ti/V ratios between 50 and 100 ($n = 75$) following the discrimination method developed by Shervais (1982; note that Shervais, 2021, recently revised the field indicating plume-derived basalts to Ti/V = 43–100); 2) for MgO within 8–16 wt% ($n = 437$) to minimize crystal fractionation and accumulation effects (cf., e.g., Jackson and Dasgupta, 2008); 3) a combination of the two, i.e., Pacific seamount compositions run through a Ti/V–MgO-filter ($n = 17$); 4) filtering for seamounts in the northern hemisphere only ($n = 1703$). In addition, we compiled compositions of seamounts located in the northwestern Pacific Ocean, east of the Izu–Bonin–Mariana subduction zone. These include data from the Magellan Seamounts (Koppers et al., 1998; Tang et al., 2019; Liu et al., 2020), the Marshall Seamounts (Davis et al., 1989), and from drill core recovery from Deep Sea Drilling Project Site 61, west of the Magellan Seamounts (Janney and Castillo, 1999), and ODP Sites 865 and 866, the Allison Guyot and Resolution Guyot at the Mid-Pacific Mountains (Baker et al., 1995). This latter compilation has 91 entries, of which we excluded the upper and lower 5% to account for outliers. Generally, most of these rocks have undergone various degrees of hydrothermal alteration; in particular the seamounts from the NW Pacific, which are up to Cretaceous in age, likely interacted with seawater over millions of years. Median compositions of the reference OIBs are presented in **Table 2**.

Theriak/Domino Thermodynamic Modeling

Equilibrium assemblage diagrams, commonly termed pseudosections, and mineral abundances were calculated using the Theriak/Domino software package, Version 15–03–2018 (de Capitani and Brown, 1987; de Capitani and Petrakakis, 2010). Calculations are based on the internally consistent thermodynamic database tcds62 from Holland and Powell

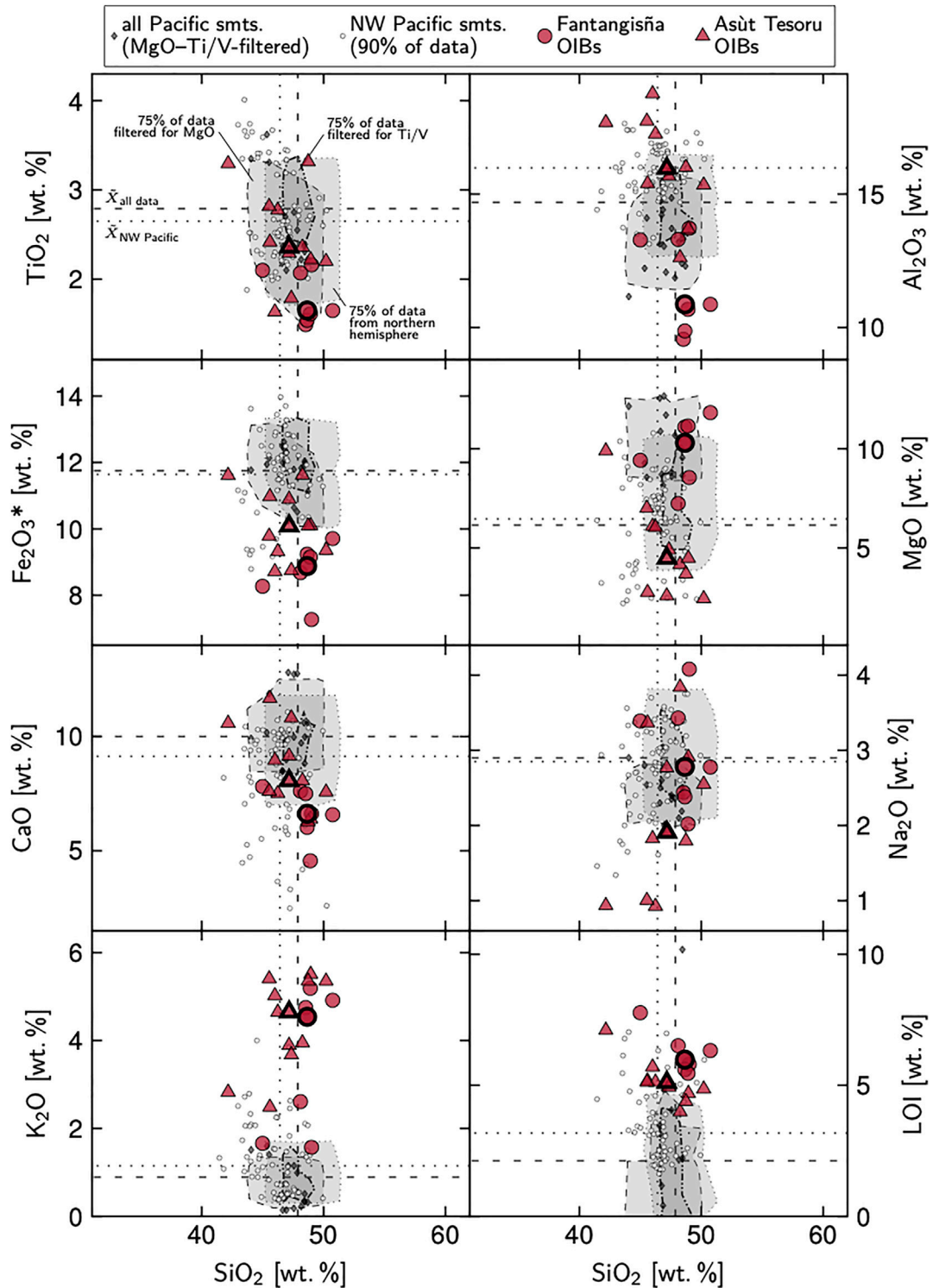


FIGURE 3 | Bulk compositions of recycled OIBs from Fantangisña and Asùt Tesoru Seamounts presented in a Harker diagram. Plot marks with thick outlines illustrate median compositions of clasts from each seamount. The clasts differ in composition (most obviously with regard to K₂O and LOI) from Pacific seamounts, implying metasomatic composition changes in the subduction zone. Data from this study, Fryer et al. (2018), and Deng et al. (2021). Compositions of Pacific seamounts are shown for comparison (see *Methods* for more information and data sources; \bar{x} = median compositions).

TABLE 1 | Summarized bulk rock compositional characteristics of the recycled OIBs.

	SiO ₂	TiO ₂	Al ₂ O ₃	Fe ₂ O ₃ *	MnO	MgO	CaO	Na ₂ O	K ₂ O	Sum	LOI
median	48.18	2.18	14.53	9.34	0.17	6.55	7.59	2.49	4.59	99.91	5.31
min	42.17	1.49	9.56	7.27	0.1	2.45	4.56	0.93	1.57	97.94	3.99
max	50.74	3.32	18.76	11.62	0.35	11.82	11.67	4.08	5.51	100.2	7.77
σ	2.04	0.54	2.73	1.12	0.06	3.11	1.77	0.93	1.28	0.64	0.92

Fe₂O₃* = FeO + Fe₂O₃; LOI, loss on ignition; σ = standard deviation = $\sqrt{(\sum (x_i - \bar{x})^2)/n}$, where x_i = observed values, \bar{x} = mean value, and n = number of analyses.

TABLE 2 | Reference bulk rock compositions of Pacific seamounts (see *OIB Reference Compositions*).

		SiO ₂	TiO ₂	Al ₂ O ₃	Fe ₂ O ₃ *	MnO	MgO	CaO	Na ₂ O	K ₂ O	LOI	Ti	V	Ti/V
All data	median	47.88	2.79	14.69	11.75	0.17	6.15	10.00	2.90	0.89	2.12	16,260	278	53.1
	σ	4.29	0.99	2.32	2.41	0.21	4.22	2.82	1.10	1.15	2.54	5,457	95.5	434.3
	<i>n</i>	2,382	2,391	2,382	2,375	2,357	2,417	2,380	2,376	2,441	7,31	2,41	1,152	152
N hemisphere	median	48.30	2.62	14.10	11.90	0.17	6.47	9.98	2.66	0.64	2.02	14,717	268	51.2
	σ	3.66	0.81	2.28	1.98	0.05	4.46	2.54	0.99	0.98	2.52	3,936	85.0	33.6
	<i>n</i>	1,291	1,292	1,289	1,291	1,291	1,291	1,289	1,293	1,326	433	143	600	128
NW Pacific	median	46.40	2.65	16.00	11.60	0.20	6.50	9.10	2.90	1.15	3.20	14,320	255	72.0
	σ	3.58	0.73	1.47	2.35	0.07	2.74	2.73	0.76	1.69	1.72	2,331	85.8	39.2
	<i>n</i>	91	84	86	74	86	86	86	86	86	74	7	85	7
MgO-filtered	median	47.49	2.38	13.00	11.64	0.17	9.96	10.11	2.36	0.49	1.03	12,660	268	49.6
	σ	2.82	0.77	1.91	1.58	0.03	1.97	2.05	0.46	0.55	2.46	4,890	47.9	10.3
	<i>n</i>	431	430	433	430	427	437	433	430	431	180	48	274	36
Ti/V-filtered	median	47.47	2.93	14.29	11.94	0.17	6.47	9.92	2.90	0.95	2.16	17,831	282	61.3
	σ	2.07	0.63	1.84	1.38	0.05	3.51	2.08	0.95	0.69	3.71	3,592	62.5	13.5
	<i>n</i>	75	75	75	75	75	75	75	75	75	55	75	75	75
MgO-Ti/V-filtered	median	47.10	2.39	13.20	11.94	0.17	10.00	9.97	2.40	0.42	3.14	15,213	273	53.7
	σ	1.22	0.43	1.04	0.68	0.01	1.45	1.38	0.30	0.50	2.69	3576	30.8	9.6
	<i>n</i>	17	17	17	17	17	17	17	17	17	9	17	17	17

Fe₂O₃* = FeO + Fe₂O₃; LOI, loss on ignition; σ = standard deviation = $\sqrt{(\sum (x_i - \bar{x})^2)/n}$, where x_i = observed values, \bar{x} = mean value, and n = number of analyses.

(2011), but we suppressed the formation of microcline, juldite (FeFe), and iron as they were not observed in the recycled OIBs. The database comes with solid solutions for olivine, ortho- and clinopyroxene, spinel, feldspar, biotite, epidote, phengite, chlorite, and chloritoid (Holland and Powell, 1998; Holland and Powell, 2003; Baldwin et al., 2005; White et al., 2007; White et al., 2014a; White et al., 2014b). It does not contain thermodynamic data for K-containing amphibole, which should theoretically result in an overemphasis of K-bearing white mica; however, K₂O contents in amphibole in the metamafics recovered from the serpentinite mud volcanoes are negligible (e.g., Table 1 in Fryer et al., 2006; SI in Ichiyama et al., 2021) so that we assume that, if at all, the overemphasis of mica is minor.

Our computations account for the oxide components SiO₂, Al₂O₃, FeO, MgO, CaO, Na₂O, K₂O, and H₂O. Equilibrium assemblage diagrams were compiled for pressure (P) = 1–10 kbar, corresponding to up to ~35 km depths when assuming an average lithospheric density of 3×10^3 kg/m³, and T = 100–600°C. Such P/T range covers the conditions of the slab beneath the Mariana serpentinite mud volcanoes but also the conditions in “warm” subduction zones (Peacock and Wang, 1999). Mineral abundances were calculated for a geotherm of 8°C/km as the equilibrium assemblage of this geotherm best overlaps with the observed mineralogy in the recycled OIBs. Diagrams were compiled for 1) the median composition of NW Pacific seamounts (Table 2), which was recalculated to Si 49.51, Al 20.09,

Fe 4.67, Mg 10.27, Ca 10.44, Na 5.90, K 1.57, and H 22.65 to use as input for Theriak/Domino, and 2) the median composition of the recycled OIB clasts (Table 1), recalculated to Si 47.60, Al 16.92, Fe 3.47, Mg 9.65, Ca 8.03, Na 4.77, K 5.79, and H 35.02. Additional O was added in both cases to account for the presence of Fe₂O₃ in the hydrothermally altered rocks.

RESULTS

Mass Balance Constraints on Compositional Changes

The major elemental compositions of the recycled OIBs reveal K₂O contents (mostly between 3.7 and 5.5 wt%) and LOI (4.0–7.7 wt%) as a proxy for H₂O that are much higher than in OIB from the Pacific Ocean (Figure 3; see also Supplementary Figure S1 for anhydrous compositions). By contrast, Fe₂O₃ and CaO in the recycled OIBs appear generally lower. Patterns in Al₂O₃, MgO, and Na₂O are inconsistent: clasts from Fantangisña appear to have less Al₂O₃, more MgO, and similar Na₂O relative to Pacific OIB whereas clasts from Asùt Tesoru have similar or higher Al₂O₃ contents but less MgO and Na₂O.

To assess the approximate changes in major element contents of the recycled OIBs, we compared them with basaltic seamounts from the northwestern Pacific (Table 2), i.e., variably altered seamounts prior to subduction at the Izu–Bonin–Mariana

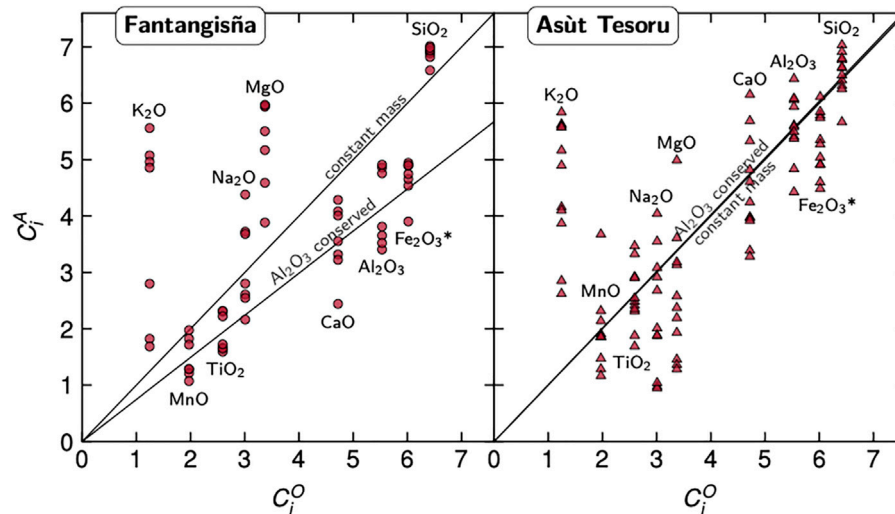


FIGURE 4 | Isocon plots comparing the anhydrous compositions of the recycled OIBs (C_i^A) to the median of the NW Pacific seamounts (C_i^O). The net mass of samples from Fantangisña Seamount appears to have increased together with gains in K_2O , SiO_2 , MgO , and Na_2O , whereas the net mass of the Asùt Tesoru Seamount samples did not significantly change and the clasts are merely enriched in K_2O and some in SiO_2 . The lines shown for Al_2O_3 -conservation are based on the mean Al_2O_3 contents; at Asùt Tesoru, the lines of constant mass and Al_2O_3 -conservation are almost identical. Oxide concentrations are scaled by the following divisors: SiO_2 , 7.5; Al_2O_3 , 3; $Fe_2O_3^*$, 2; MnO , 0.1; MgO , 2; CaO , 2.

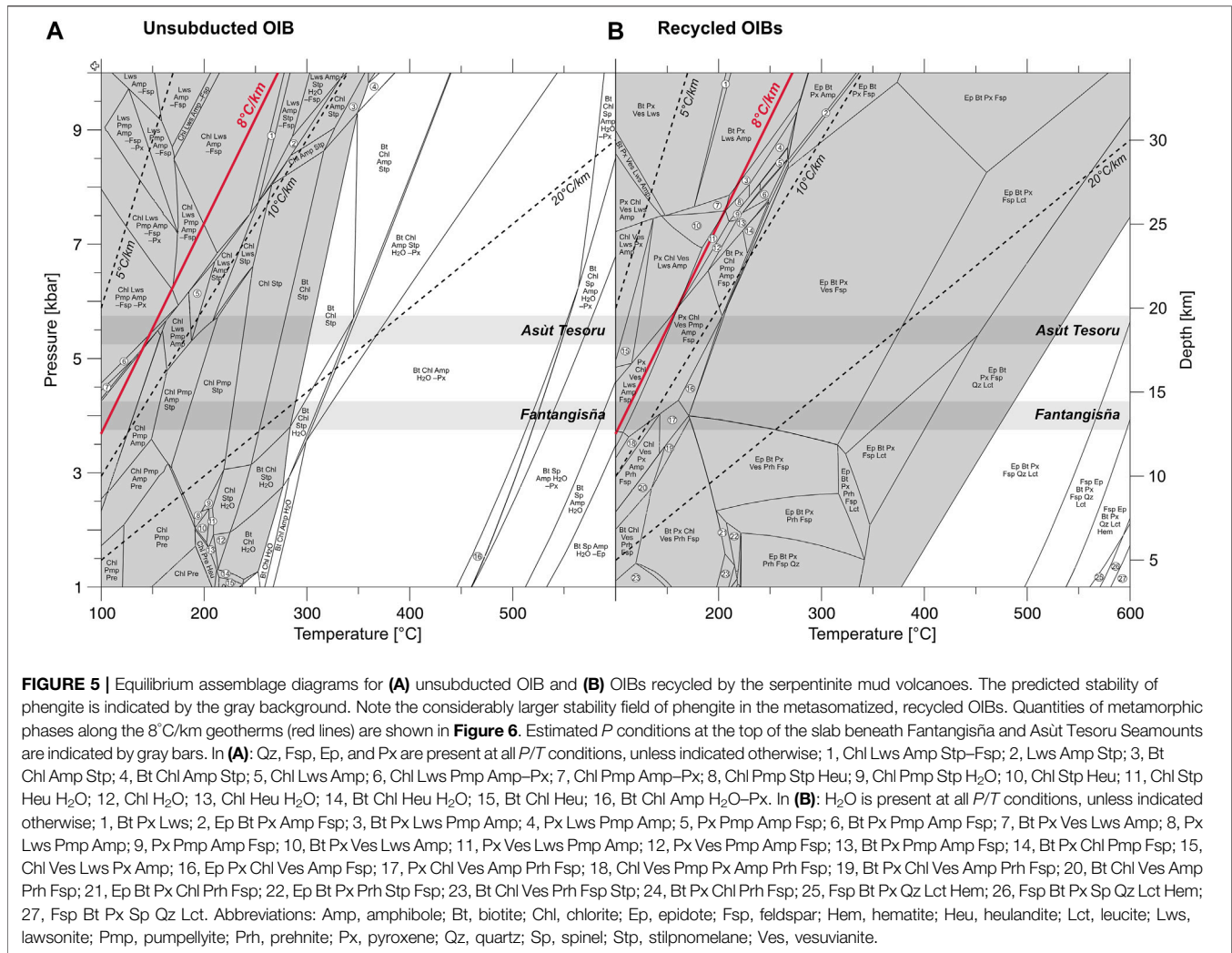
TABLE 3 | Results of isocon analysis, relative to OIB from the NW Pacific (cf. **Table 2**), assuming the conservation of Al_2O_3 .

Sample	Mud volcano	Reference	SiO_2	TiO_2	Al_2O_3	$Fe_2O_3^*$	MnO	MgO	CaO	Na_2O	K_2O
U1497A-8F-2, 14–17 cm	Fantangisña	Deng et al. (2021)	1.17	1.01	1.00	0.86	1.14	1.75	1.03	1.41	1.67
U1497A-11G-CC, 22–25 cm	Fantangisña	Deng et al. (2021)	1.23	1.01	1.00	0.73	1.04	1.53	0.85	1.64	1.53
U1497A-12F-1, 78–81 cm	Fantangisña	Deng et al. (2021)	1.25	1.00	1.00	0.90	1.01	1.34	1.01	1.42	2.62
U1498B-23R-1, 60–63 cm	Fantangisña	Deng et al. (2021)	1.75	1.00	1.00	1.28	1.06	2.65	1.38	1.41	6.62
U1498B-23R-1, 67 cm	Fantangisña	this study	1.61	0.97	1.00	1.23	0.93	2.68	1.06	1.41	6.03
U1498B-23R-1, 67–69 cm	Fantangisña	Deng et al. (2021)	1.70	1.00	1.00	1.29	1.02	2.77	1.07	1.33	6.13
U1498B-23R-1, 70–75 cm	Fantangisña	Deng et al. (2021)	1.58	0.96	1.00	1.18	0.79	2.57	0.75	1.04	6.48
U1496B-8X-CC, 0–2 cm	Asùt Tesoru	Deng et al. (2021)	1.32	1.20	1.00	1.27	0.93	0.81	1.12	1.68	4.17
U1496B-8X-CC, 0–4 cm	Asùt Tesoru	Fryer et al. (2018)	1.02	1.00	1.00	0.98	0.96	0.44	1.33	1.21	2.15
U1496B-8X-CC, 8–13 cm	Asùt Tesoru	Fryer et al. (2018)	1.02	0.92	1.00	0.94	0.96	0.40	1.01	0.96	3.25
U1496B-8X-CC, 30–32 cm	Asùt Tesoru	Fryer et al. (2018)	1.13	0.92	1.00	0.84	0.67	0.39	0.87	0.92	4.65
U1496B-8X-CC, 33–41 cm	Asùt Tesoru	Deng et al. (2021)	1.23	1.04	1.00	1.02	0.68	0.81	0.82	1.17	5.37
U1496B-10F-2, 0–5 cm	Asùt Tesoru	Fryer et al. (2018)	1.05	1.33	1.00	0.87	1.85	0.57	0.69	0.62	4.46
U1496B-10F-2, 5–8 cm	Asùt Tesoru	Fryer et al. (2018)	1.04	0.73	1.00	0.77	1.09	0.77	1.21	0.67	3.13
U1496B-10F-2, 13 cm	Asùt Tesoru	this study	0.85	0.56	1.00	0.64	0.81	0.80	0.84	0.54	3.57
U1496B-10F-2, 14 cm	Asùt Tesoru	this study	0.89	1.02	1.00	0.76	0.85	0.97	0.75	0.31	4.07
U1496B-10F-2, 17–20 cm	Asùt Tesoru	Fryer et al. (2018)	0.92	1.03	1.00	0.74	0.87	0.86	0.77	0.30	3.59
U1496B-10F-2, 35 cm	Asùt Tesoru	this study	0.82	1.19	1.00	0.91	1.10	1.38	1.05	0.29	2.13

$Fe_2O_3^* = FeO + Fe_2O_3$; LOI, loss on ignition.

subduction system (referred to as “unsubducted OIB” from here on). It can be expected that the recycled OIBs were compositionally similar to these unsubducted OIB prior to subduction. Results of our isocon analysis (Gresens, 1967; Grant, 1986) are shown in **Figure 4**; calculations were done on an anhydrous basis. The results imply the addition of K_2O and variable amounts of SiO_2 to clasts from both seamounts and of MgO to OIBs from Fantangisña when constant mass is assumed. The assumption of constant mass appears reasonable for Asùt Tesoru where TiO_2 and Al_2O_3 , both considered rather immobile at shallow subduction levels (e.g., Manning, 2004), lie on the

isocon line. At Fantangisña, however, this assumption would suggest the loss of all immobile species—which is unlikely. We hence calculated additional isocon lines assuming the conservation of Al_2O_3 (**Figure 4** and **Table 3**). The median slope of these isocon lines at Asùt Tesoru ($y = 1.006x$) is almost identical to the one assuming constant mass ($y = x$). It is, by contrast, much less steep at Fantangisña ($y = 0.747x$); we argue that this assumption is reasonable here since the immobile TiO_2 plots well on this line of Al_2O_3 conservation. It hence appears 1) that a net increase in mass affected the clasts from Fantangisña but not from Asùt Tesoru and 2) that the recycled



OIBs from Fantangisña gained K_2O , SiO_2 , MgO , and Na_2O whereas those from Asút Tesoru gained K_2O and some SiO_2 but lost Fe_2O_3 and possibly MgO . The bulk of these changes can likely be ascribed to metasomatic processes that accompanied fluid-rock interactions within the subduction system (see Discussion).

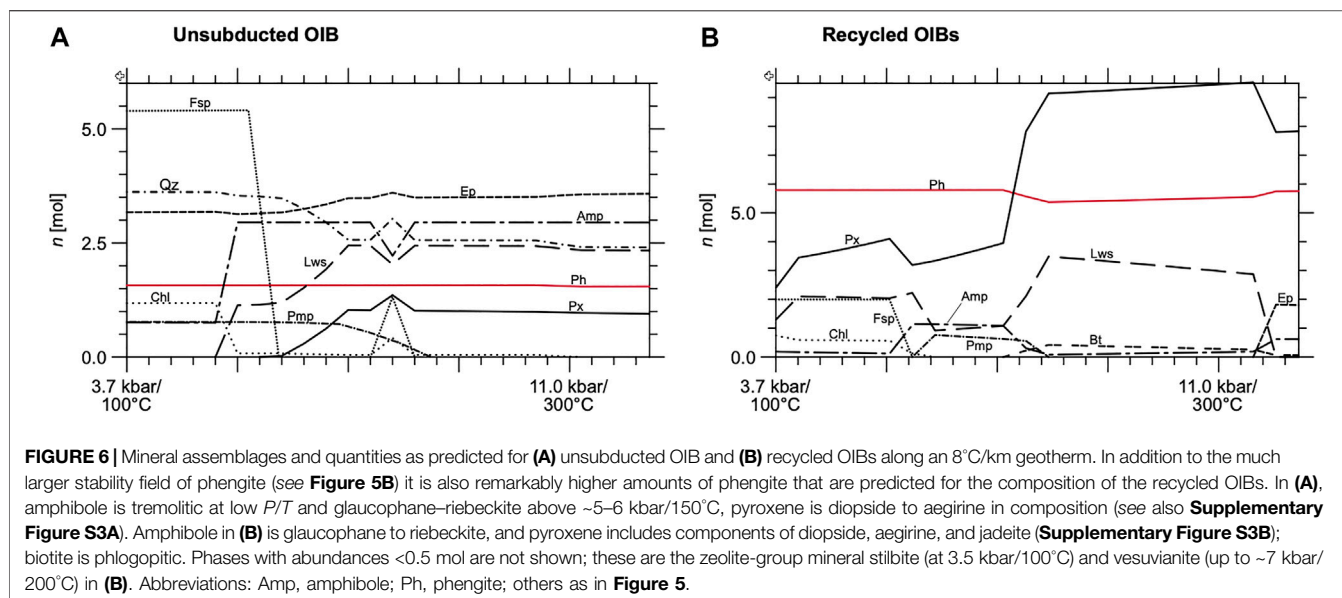
Equilibrium Assemblage Diagrams

Equilibrium assemblage diagrams compiled for the median compositions of unsubducted OIB and the recycled OIBs illustrate which mineral phases are to be expected in these rocks. The section for the unsubducted OIB thereby serves as a reference to determine the mineralogical consequences induced by the compositional changes that we ascribe to fluid-metasomatism.

For the unsubducted OIB, quartz, feldspar, pyroxene, epidote, and chlorite are predicted to be stable throughout most of the modeled P/T conditions (Figure 5A). Prehnite may form below ~ 3 kbar/ $200^\circ C$. At higher T , biotite and tremolitic amphibole become part of the mineral assemblage. Pumpellyite exists at low T and up to ~ 10 kbar, together with riebeckitic amphibole and

lawsonite at $P > \sim 3$ kbar. Glaucophane amphibole joins the assemblage at ~ 4.5 kbar/ $100^\circ C$, persisting between ~ 200 and $300^\circ C$ to higher P . Phengite is restricted to $T < 350^\circ C$. The equilibrium assemblage predicted for the recycled OIBs strongly differs from this (Figure 5B). Quartz is absent except for low- P /high- T conditions, tremolite is not predicted at all, and epidote will not form at $T < 200^\circ C$. Biotite is present throughout the model conditions, except for intermediate P and $T < \sim 200^\circ C$. Prehnite exists up to ~ 4 kbar/ $350^\circ C$, vesuvianite may form at T up to $450^\circ C$, and the stability field of pumpellyite is restricted. Riebeckite and glaucophane form at > 2 kbar/low T , and lawsonite at high P /low T . Phengite is stable throughout most of the modeled P/T range.

In unsubducted OIB, the equilibrium assemblage along the $8^\circ C/km$ geotherm is dominated by feldspar, quartz, and epidote until ~ 6 kbar/ $150^\circ C$, accompanied by minor chlorite and pumpellyite (Figure 6A). Lawsonite and amphibole contents increase at $T > 150^\circ C$ and at 170 – $200^\circ C$ the amount of pumpellyite decreases whereas that of pyroxene increases. Amphibole is tremolitic to riebeckitic below ~ 6 kbar/ $150^\circ C$, and mainly glaucophane at higher P/T conditions



(Supplementary Figure S3A). Above ~7 kbar/200°C, the mineral assemblage consists of epidote, amphibole, quartz, lawsonite, and pyroxene (mainly diopsidic in composition; Supplementary Figure S3A). About 1.5 mol of phengite exists throughout the prograde path. Contrastingly, with 5–6 mol phengite and >3–4 mol pyroxene present along the 8°C/km geotherm, these two phases dominate the mineral assemblage in the recycled OIBs (Figure 6B); above 200°C, pyroxene contents even increase to ~9 mol. Diopside and aegirine components in pyroxene are predicted below 200°C, and jadeite pyroxene joins this assemblage at higher P/T conditions (Supplementary Figure S3B). Lawsonite is stable even at 3.5 kbar/100°C but is most abundant at $T > 200^\circ\text{C}$. Minor amounts of riebeckitic amphibole are formed at $T < 200^\circ\text{C}$ and moderate to minor amounts of glaucophane at $T > 150^\circ\text{C}$ (Supplementary Figure S3B). Chlorite and feldspar exist up until 6 kbar/160°C, and the presence of pumpellyite is restricted to ~160°C at 6 kbar and 220°C at 8 kbar. Up to ~7 kbar/200°C, minor amounts of vesuvianite are predicted; in case vesuvianite is not allowed to form in the models, pyroxene and pumpellyite contents increase at $T < 200^\circ\text{C}$ whereas the lawsonite content decreases (see Supplementary Figure S4 and discussion in the figure caption).

DISCUSSION

Transfer of Mass Within the Mariana Forearc Subduction Metasomatism vs. Seafloor Alteration Processes

It has long been known that subduction zones are sites of major mass transfer and chemical cycling. The meta-OIB data reported by Fryer et al. (2018), Deng et al. (2021), and in this study provide direct evidence for mass transfer at shallow levels of the Mariana convergent margin. Most striking are increases in K_2O and LOI,

but our mass balance calculations imply that SiO_2 , MgO , and Na_2O are also modified (Figure 4 and Table 3).

In general, subducting lithologies undergo prograde metamorphic phase changes in response to rising P and T with increasing depth. Such transformations could (theoretically) occur in geochemically closed systems, in which the phase assemblages of the subducting lithologies would change but the bulk rock would retain its composition. Contrastingly, fluid-induced metasomatism can lead to the transfer of mass into or away from individual pieces of rock, modifying their bulk composition. Absolute increases in certain elements should hence be mainly the result of the interaction with fluids that transported the respective elements; losses in element concentrations are usually ascribed to the breakdown of out-of-their-stability-field minerals and the fluid-mediated removal of the released elements (e.g., Putnis and Austrheim, 2010).

Quantitatively assessing the compositional changes of the recycled OIBs is difficult because their exact compositions prior to subduction are unknown. It can be assumed that they were generally similar to OIB situated in the northwestern Pacific Ocean—but the compositions of such vary to a certain degree as analyzed sample suites usually cover a range of primary and secondary processes (such as magmatic differentiation and crystal accumulation effects or hydrothermal alteration; cf. Figure 3; see also Supplementary Figure S2). The problem of attributing compositional changes to fluid-rock interactions within the subduction zone becomes particularly clear when considering, for instance, MgO contents in the recycled OIBs of which most overlap with that of the unsubsucted OIB (Figure 3 and Supplementary Figure S1). The relatively higher values at Fantangisña (median = 10.3 wt% vs. 4.5 wt% at Asút Tesoru) could potentially be explained by the aforementioned primary or secondary processes. Indeed, when compared to the MgO-Ti/V -filtered data of all Pacific seamounts, some samples contain up to ~12 wt% MgO (gray diamonds in Figure 3). By contrast, K_2O

contents of the recycled OIBs (median = 4.5 wt% at Fantangisña and 4.7 wt% at Asùt Tesoru) clearly exceed those of unsubsucted seamounts (up to 4 wt%; median = 1.15 wt%) so that it appears very unlikely that these enrichments have been induced prior to subduction. Similarly, we argue that SiO₂ (median = 48.2 wt% in the recycled OIBs; median = 50.9 wt% on an anhydrous basis) has been added to most clasts during subduction: hydrothermal alteration of basalts at the seafloor admittedly also increases SiO₂ (e.g., Staudigel et al., 1996) and similar contents in unsubsucted OIB are not uncommon (50% of data between 44.6 and 47.2 wt%; **Figure 3** and **Supplementary Figure S1**), but the observed gains in K₂O and H₂O would dilute these values to <<46 wt%. Our isocon analysis further imply that Na₂O was gained in the OIBs from Fantangisña whereas Fe₂O₃* was lost from those from Asùt Tesoru (**Figure 4**).

Altogether, it cannot be excluded that some of the differences between unsubsucted and recycled OIBs represent a sampling bias and/or seafloor alteration processes. But in particular the increases in K₂O and H₂O, as well as, to a lesser extent, SiO₂ and Na₂O can presumably be attributed to fluid-metasomatism during subduction. This transfer of mass can be well explained by the presence of solute-laden fluids in the Mariana forearc that are particularly abundant and well documented (e.g., Mottl et al., 2004; Savov et al., 2007; *see below*). The lateral distance of >160 km between the Fantangisña and Asùt Tesoru Seamounts, together with the fact that K₂O–SiO₂-enriched OIBs were recycled at both sites, suggests that the metasomatic processes are not a local phenomenon but are widespread in the Mariana subduction system.

Shallow Subduction Fluid Processes and OIB Alteration

Fluid and solute release following mineral breakdown reactions in the subducting slab can be traced at the outer Mariana forearc by slab-derived fluids that expel at the serpentinite mud volcano summits. The compositions of these slab-derived fluids systematically change across the forearc, in response to prograde metamorphic processes at depths of ~10–30 km and $T = <80\text{--}350^\circ\text{C}$ (e.g., Mottl et al., 2004; Savov et al., 2007; Hulme et al., 2010; Fryer et al., 2018). The inferred processes in the slab range from sediment compaction and opal-CT dehydration at shallowest levels to clay diagenesis and dehydration, the release of desorbed water, and decarbonation at greater depths (Mottl et al., 2004; Hulme et al., 2010; Menzies et al., 2021). The decarbonation of subducted sediments and AOC (altered igneous portions of the oceanic crust), for example, is thought to result in high carbonate alkalinity in slab-derived fluids of the deeper-sourced mud volcanoes relative to shallow-sourced ones. High alkalinity in turn favors the precipitation of CaCO₃ below the deep-sourced mud volcanoes, leading to a depletion of Ca and Sr in the fluids that rise to the forearc seafloor. By contrast, Ca and Sr in pore waters at the shallower-sourced mud volcanoes are enriched because the slab is still too cold for decarbonation to occur (Mottl et al., 2004). Expressed in numbers, Ca decreases from >50 mmol/kg to <1 mmol/kg and Sr from >500 μmol/kg to <20 μmol/kg across the forearc (*see compilations in Wheat et al., 2018; Menzies et al., 2021*). Similarly, K, Rb, Cs, and B

are thought to be leached from the subducted sediments and AOC once the slab has warmed to $T > 100\text{--}150^\circ\text{C}$ (Mottl et al., 2004; Hulme et al., 2010). Concentrations of these in the serpentinite mud pore waters as a result increase from shallow- to deep-sourced sites. Potassium changes from <1 mmol/kg to >15 mmol/kg, Rb increases from <1 μmol/kg to >5 μmol/kg, Cs from <5 nmol/kg to >>50 nmol/kg, and B from <1 μmol/kg to >3,000 μmol/kg (Wheat et al., 2018). Contents of Si are generally low in the serpentinite mud pore waters (Geilert et al., 2020) since Si is readily taken up by the forearc mantle peridotite during serpentinitization (e.g., Albers et al., 2020; Geilert et al., 2021). But Si contents in slab-fluids were likely much higher shortly after their release as originating, for instance, from opal diagenesis and/or the transformation of smectite to illite (cf., e.g., Mottl et al., 2004; Kastner et al., 2014).

In the subduction channel, comminuted material as well as rock clasts react with these fluids. Serpentinites, previously entitled “sponges” for fluid-mobile elements (Deschamps et al., 2011), can contain high concentrations of Rb, Cs, B, and other fluid-mobile elements (e.g., Debret et al., 2019; Albers et al., 2020). Contents of K₂O in the serpentinite clasts and mudflows are, however, low with on average <<0.1 wt% (e.g., Savov et al., 2005a; Savov et al., 2005b)—despite the general availability of K at the deeper-sourced mud volcanoes (*see above*). This is presumably the case because serpentinite phases do not incorporate K in their structure. In consequence, the forearc serpentinite does not act as a sink for K. Following this line of thought, K-containing fluids are likely available to react with any lithology in the subduction channel that could form K-bearing minerals. Such lithologies encompass subducted mafics, including OIB, which provide the components and the chemical environment to form phengite or biotite.

The uptake of K has been mostly pervasive, as evidenced by the abundant replacement of former groundmass by phengite in the recycled OIBs (**Figure 6** in Fryer et al., 2020) and the shortage of K-bearing phases in metamorphic veins (Albers et al., 2019). Indeed, no such phases have been observed in veins of OIBs recycled at Fantangisña. In addition, we generally observed less phengite in the samples from Fantangisña and also little other K-bearing minerals so that it remains somewhat enigmatic which phases account for the strong K₂O increase.

Likewise, the differences in metasomatic element uptake between the clasts from Fantangisña and Asùt Tesoru (**Figure 4**) are to some extent questionable and cannot unequivocally be clarified in this study. The recycled OIB clasts from both sites should, theoretically, have experienced similar P/T paths as well as interactions with similar slab-fluids when assuming 1) homogeneous compositions of the incoming crust and 2) similar exposure times to slab-fluids in the subduction channel. But OIBs from Fantangisña, the shallower-sourced seamount, are marked by a net increase in mass and uptake of K₂O, SiO₂, MgO, and Na₂O and those from the deeper-sourced Asùt Tesoru show increases in K₂O and SiO₂ and possibly losses of MgO and Fe₂O₃*. Given these distinctions, we follow that 1) and/or 2) are incorrect. But even when considering variations of the subducting lithosphere at the two sites (being >160 km apart) it is difficult to explain the loss in

MgO (and Fe₂O₃*) in the Asùt Tesoru OIBs, since the subduction channel mélange, the mud volcano conduits, and the mudflows in which the clasts resided are overall characterized by ultramafic, Mg–Fe-rich materials. The second possibility would be that the exposure times of the Asùt Tesoru samples within the Mg-rich environment were much shorter as compared to the Fantangisña OIBs, but similar enrichments in K₂O between the two sites suggest otherwise. In contrast, the addition of MgO (and maintenance of Fe₂O₃*) in the samples from Fantangisña appears plausible in this overall ultramafic environment; comparably, MgO contents in seafloor basalt typically increase as a result of hydrothermal alteration and chlorite formation at similar *T* (e.g., Staudigel et al., 1996; Bach et al., 2013). The gain in SiO₂ in samples from both mud volcanoes presumably occurred in a pervasive manner—we assume that slab-fluids have initially been siliceous (*see above*)—but may in addition be explained by the presence of silicates in metamorphic veins: pectolite, prehnite, white mica, and lawsonite occur at both study sites (Albers et al., 2019). Pectolite, NaCa₂Si₃O₈(OH), however, appears to be more frequent in OIBs from Fantangisña, which partly explains the Na₂O increase in these samples. Further, plagioclase feldspar in these samples may be Na-rich as is typical for hydrothermally altered seafloor basalts (Alt, 1995). Feldspar is predicted to be stable at rather low *P/T* along the 8°C/km isotherm (**Figure 6B**), which could indicate that it is part of the equilibrium assemblage in clasts from Fantangisña but not in those from the deeper-sourced Asùt Tesoru. In the latter, the replacement of plagioclase by lawsonite and phengite (*see Figure 6* in Fryer et al., 2020) lends further credence to this idea. During this process, some of the Na from the plagioclase's albite component is possibly being released from the rocks and hence explains the clasts' lower Na₂O contents. After all, aside from heterogeneities in the composition of the subducting crust, it may be this and similar breakdown reactions/changes in mineral stabilities that explain the variations between the OIBs from the two mud volcanoes that tap different *P/T* conditions in the subduction channel.

Mariana Forearc *P/T* Conditions and Ramifications of Metasomatism for Mineral Stabilities

The observed compositional changes have direct implications for the thermodynamic stability of mineral phases. This is most striking for the stability field of phengite that is limited to <300°C in unsubducted OIB but, for the metasomatized ones, is increased to 600°C at both cold and warm subduction zones (**Figure 5**). In addition, besides this larger stability field, considerably larger quantities of phengite (~6 instead of ~1.5 mol; **Figure 6**) are being predicted for the metasomatized OIBs.

The exact geotherm and the respective *P/T* conditions in the Mariana subduction system remain vague. The depth to the slab below the mud volcanoes—from which *P* can be derived—could relatively well be determined using multi-channel seismic reflection data (e.g., Oakley et al., 2008). But estimates on *T* conditions are less precise because they chiefly rely on interpretations of equilibrium mineral assemblages and mineral compositions in metamafic clasts (e.g., Maekawa et al.,

1993; Oakley, 2008), on across-forearc changes in pore water compositions of the serpentinite mud (e.g., Mottl et al., 2004; Menzies et al., 2021), and on oxygen stable isotope compositions of serpentine–magnetite pairs. The serpentine–magnetite pairs, for instance, imply serpentinitization *T* of up to 400°C for samples from Asùt Tesoru Seamount (Debret et al., 2019), whereas metamafic mineral assemblages and compositions imply *T* of 200–250°C for that seamount (Ichiyama et al., 2021). To make matters worse, the travel paths from depths to the forearc seafloor are not completely understood; several authors have suggested that both metamafic and serpentinite clasts may travel upwards in the subduction channel after having been subducted to greater depths (e.g., Tamblyn et al., 2019) and before being entrained by mud volcanism. They could hence have experienced metamorphic conditions greater than those right below the individual mud volcanoes. In this sense, a blueschist clast from South Chamorro Seamount was interpreted to have experienced up to 19 kbar and 590°C (Tamblyn et al., 2019).

Pressure at the slab is despite these uncertainties estimated at ~4 kbar below Fantangisña (~14 km slab depth) and 6 kbar below Asùt Tesoru (~18 km; Oakley et al., 2008), with *T* of ~150 and 250°C, respectively. Resultant geothermal gradients would span a range of 10–14°C/km, or even 6–17°C/km when including the *P/T* estimates for the other serpentinite mud volcanoes (*see, e.g., Table 1* in Fryer et al., 2020). This large range may be explained by inaccuracies introduced by various factors. For instance, the complex topography of the subducting Pacific Plate implies a high relief of the slab–wedge interface (Fryer et al., 2020) and it is possible that topographic highs such as subducted seamounts cause seismic reflections that are interpreted as the top of the subducting slab; these may, however, protrude from the surrounding subducting seafloor by several kilometers and hence affect the depth estimates. Temperature estimates on the other hand, in particular the ones based on metamorphic mineral assemblages, may be biased by the time the metamorphism occurred. Shortly after the subduction initiation in the Eocene, the mantle wedge was much hotter than today, which lead to higher-grade metamorphism at a given depth of the subduction channel than today (Ichiyama et al., 2021). In support of this, age-dating metamorphic minerals in a blueschist clast from South Chamorro Seamount revealed a formation age of >45 Ma (Tamblyn et al., 2019).

The geotherm of ~8°C/km appears to be best consistent when comparing the observed mineral assemblages (Albers et al., 2019; Fryer et al., 2020; Deng et al., 2021; Ichiyama et al., 2021) with our equilibrium assemblage diagrams (**Figure 5B**). Along this geotherm, jadeitic pyroxene joins the metamorphic assemblage at ~7 kbar/200°C (**Supplementary Figure S3B**), which would be the minimum *P/T* conditions the clasts at Asùt Tesoru Seamount have experienced. The key criterion for the 8°C/km geotherm is the presence of lawsonite, which is not predicted for steeper geotherms, e.g., of 10°C/km (dashed line in **Figure 5B**). Following this argument, the lack of lawsonite in OIBs from Fantangisña Seamount implies *P* ≤ 4 kbar—which would further implicate ~100°C when following the 8°C/km geotherm. The *T* the OIBs experienced was, however, likely higher as suggested by the

presence of pumpellyite that is restricted to 160–220°C. It must be kept in mind though that the computed phase diagram applies to the recycled OIB's median composition. Due to compositional differences between individual clasts and between Fantangisña and Asùt Tesoru, (minor) deviations between the predicted and the observed mineral assemblages and their compositions are not unlikely. For example, amphibole is predicted to be mainly glaucophane above ~5.5 kbar/150°C, with a limited riebeckite component; lower MgO in the clasts from Asùt Tesoru relative to those from Fantangisña (**Figure 3**) would potentially decrease the glaucophane fraction in amphibole. Allowing, during thermodynamic modeling, only for the formation of amphibole with compositions similar to those observed by Ichiyama et al. (2021), i.e., $\text{Rbk}_{0.65}\text{Gln}_{0.35}$, results in a very similar mineral assemblage (**Supplementary Figure S5**). The amount of amphibole, however, is lower in particular at intermediate P/T at which higher amounts of pyroxene are instead predicted, and pumpellyite is stable up to somewhat higher P/T conditions. The predicted pyroxene compositions (similar amounts of the aegirine and jadeite components; **Supplementary Figure S6**) are also similar to those analyzed by Ichiyama et al. (2021). Further, the lower bulk Al_2O_3 in the OIBs recycled at Fantangisña (median = 10.9 wt% vs. 16.0 wt% at Asùt Tesoru; **Figure 3**) may explain lower amounts of phengite (Albers et al., 2019; Ichiyama et al., 2021) in clasts from this mud volcano, since Al is an important constituent in the muscovite component of phengite.

Aside from the compositional variability, the metasomatism of the clasts is a continual process: they react with fluids with evolving solute loads (in response to increasing P/T conditions) while being dragged to greater depths. Some of the metasomatism likely occurred at relatively late stages, i.e., after the subduction to and metamorphism of the (at that time only partly metasomatized) OIB clasts at a certain depth. As metamorphic reactions can be considered generally rather sluggish at the considered P/T range, the clasts' equilibration with the ever-evolving slab-fluid should lag behind and P and T overstepping may be needed for the reactions to proceed (e.g., Pattison et al., 2011). This assumption is supported by the presence of vein mineralogies in the metamafics that are distinct from the phase assemblages in the clast's groundmasses. Sodic amphibole, pumpellyite, and chlorite for example replace Na pyroxene or the igneous groundmass (Ichiyama et al., 2021) but have not been observed in veins that formed in apparent equilibrium with the slab-derived fluids in the subduction channel (Albers et al., 2019). It would hence be possible that phases such as lawsonite formed in the subducted OIBs before the rocks were metasomatized to their current compositions.

Taken together, a reasonable consensus between observations and models exists. However, reproducing the metamorphic phase assemblages by equilibrium modeling is impeded by compositional variabilities, the timing of the metasomatism, and potentially by partial out-of-equilibrium states of the clasts. We estimate the geothermal gradient at 8–10°C/km, whereby the lower gradient appears realistic for today's mature subduction zone in which mantle wedge has been cooled by the

>180 My old subducting Pacific Plate since the Eocene. Metamorphism in the geologic past may have occurred at higher T . Our model results hence strengthen previous studies suggesting ~4 kbar/up to 160–220°C for the OIBs recycled *via* the Fantangisña mud volcano and up to 7–8 kbar/200–350°C for those from Asùt Tesoru. The metasomatic changes in bulk composition markedly increase the stability field of phengite.

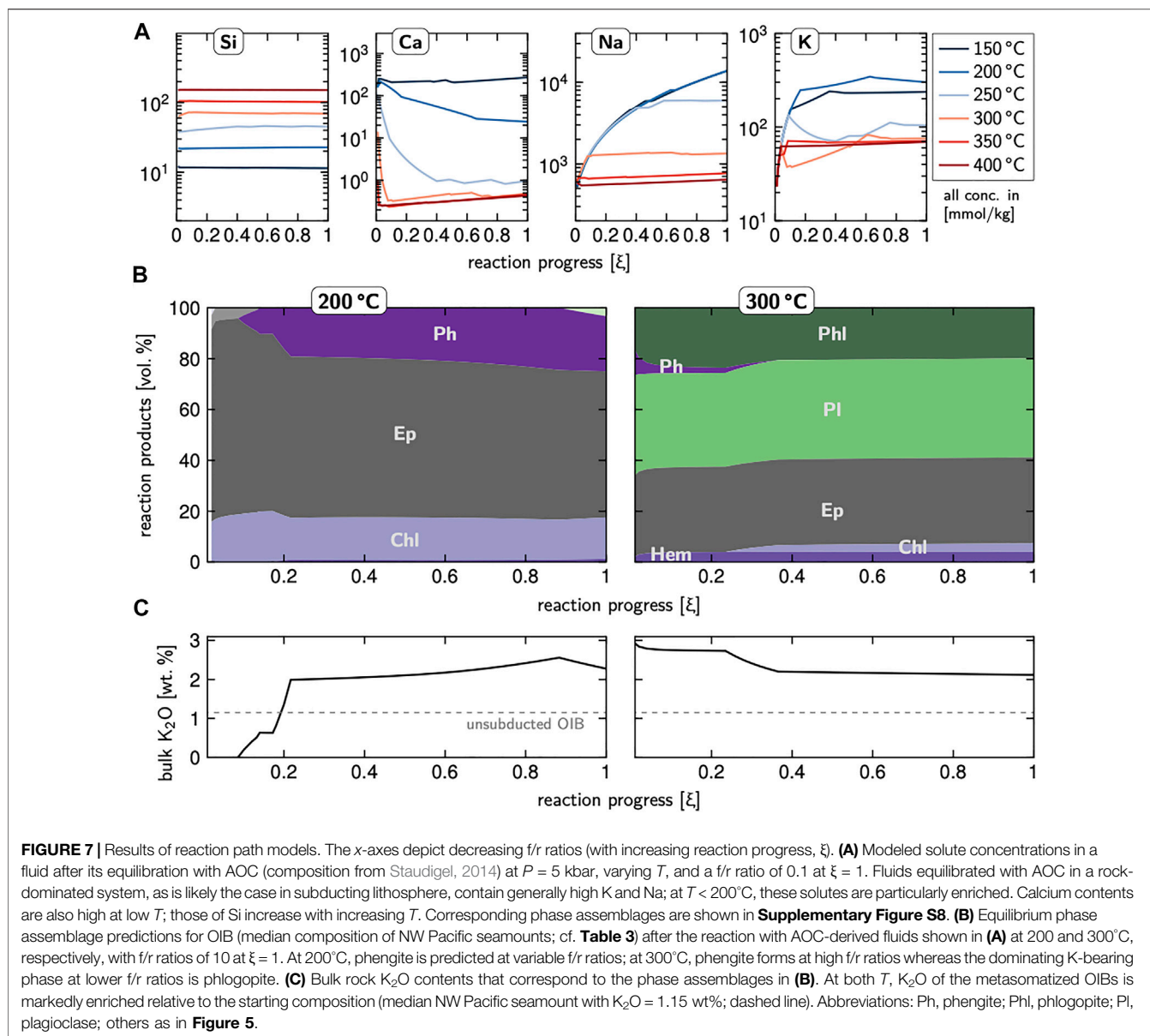
Reaction Path Modeling Constraints on Metasomatism at Shallow Depths

We carried out thermodynamic reaction path modeling to better understand the fluid–rock reactions in the subduction channel and the most obvious metasomatic changes, i.e., the transfer of K_2O from the subducting slab into OIB. The models are thought to provide a generalized view of mass transfer at subduction depths of 15–20 km.

Sediments being subducted at the Mariana Trench consist of chert, radiolarite, volcanic turbidites, and pelagic clay, of which only the turbidites and clay contain significant amounts of K_2O (up to ~1.9 wt% and 3.9 wt%, respectively; Plank and Langmuir, 1998). The limited thicknesses of these units east of the Mariana Trench (190–220 m and 40–80 m, respectively; Plank et al., 2000) restrict the overall amounts of K_2O that can be liberated from these. The other main source for K_2O in the slab-derived fluids is subducting AOC. At a global scale, AOC has on average 0.65 wt% K_2O (Staudigel, 2014) but contents in the Cretaceous basalts east of the Mariana Trench can exceed 5 wt% (ODP Site 801, the recovery of which does, however, not necessarily represent “typical” altered AOC as it contains a silicic hydrothermal deposit; Kelley et al., 2003). The igneous basement is hundreds of meters thick, providing a vast reservoir for K_2O .

As starting compositions in the models, we used the bulk sediment composition from east of the Mariana Trench, AOC (the conservative composition with 0.65 wt% K_2O), and a 50:50 mixture of the two. The modeling consists of two steps: 1) to approximate the composition of the fluid that is released from the slab, we equilibrated sediments, AOC, and the 50:50 mixture, respectively, with a fluid at $P = 5$ kbar, varying T (150–400°C in 50°C steps), and a final fluid/rock mass ratio (f/r ratio) of 0.1; 2) to mimic fluid–rock reactions in the subduction channel, we reacted a median NW Pacific OIB composition (**Table 2**) with the fluid resulting from 1), at $P = 5$ kbar, $T = 200$ and 300°C, and a final f/r ratio of 10. Details on the models and thermodynamic data are provided in the **Supplementary Information**.

Modeling results of the AOC–OIB runs are summarized in **Figure 7**; results from the other setups are presented in **Supplementary Figure S7**. In all cases, K as well as Si, Ca, and Na are mobilized from the starting lithologies (**Figure 7A** and **Supplementary Figure S7A**). Solute concentrations in the fluids are, however, strongly dependent on T and partly dependent on the f/r ratio; concentrations can vary by a factor of 10 and more. The corresponding mineral assemblages predicted for the subducted slab are shown in **Supplementary Figure S8**. Upon the reaction of the solute-laden fluids with OIB, mineral assemblages are dominated by epidote, phengite, and chlorite at 200°C with abundant lawsonite at fluid-dominated and



quartz at more rock-dominated conditions when the fluid is (partly) sourced in subducting sediment (**Figure 7B** and **Supplementary Figure S7B**). At 300°C, plagioclase, epidote, and phlogopite characterize the equilibrium assemblage in the model runs following AOC and AOC–sediment equilibration, with minor hematite, chlorite, and phengite at high f/r ratios. By contrast, the sediment–OIB models predict dominantly quartz and garnet together with talc and stilpnomelane (at high f/r ratios) and chlorite (towards lower f/r ratios). Bulk K_2O contents in the now metasomatized OIBs have approximately doubled over most of the model conditions at 200°C, now exceeding 2 wt% except for strongly fluid-dominated systems and towards completed reaction in the sediment–OIB runs (**Figure 7C** and **Supplementary Figure S7C**). At 300°C, K_2O even approaches 3 wt% in the AOC–OIB models whereas a loss of K_2O from the OIB is predicted for the sediment–OIB models. The major hosts

of K_2O are phengite and phlogopite at 200 and 300°C, respectively.

Our modeled fluid compositions are generally consistent with observations from the serpentinite mud volcanoes in that they imply considerable mobilization of mass from the slab at shallow depths and low T . The fluids in the Mariana forearc, however, undergo severe compositional changes during the reaction with solids in the subduction channel and during their rise to the forearc seafloor (e.g., loss of Si and Ca; see *Shallow Subduction Fluid Processes and OIB Alteration*), so that the modeled fluid compositions cannot directly mirror those recorded in the serpentinite mud pore waters. But, for instance, the presence of abundant prehnite and pectolite with equilibrium growth structures in metamorphic veins in the recycled OIBs (Albers et al., 2019) lends strong credence to the existence of Si–Ca–Na–K-containing fluids. Further, the corresponding

phase assemblages in the fluid source lithologies (**Supplementary Figure S8**) appear reasonable for the physicochemical (modeling) conditions: comparable assemblages were described as alteration products in mafic rocks and/or sediments that experienced metamorphism up to blueschist grade overprints (e.g., Ernst, 1984; Jayko et al., 1986). Phases predicted to be stable in the metasomatized OIB (**Figure 7C** and **Supplementary Figure S7C**) resemble those in metabasaltic rocks that were interpreted to have reacted with slab-derived fluids at shallow subduction levels, such as greenstones and blueschists from the Franciscan Complex (e.g., Bebout and Barton, 1993; Ukar and Cloos, 2014).

It must be kept in mind, however, that our models oversimplify the natural system by assuming complete chemical equilibrium between all reactants, by not including kinetic effects, as well as by limitations of thermodynamic data at low T and a possible shortage of relevant low- T mineral phases in the database. The models cannot emulate the vast complexity of natural reactions taking place in subduction zones, which are influenced by factors such as the physicochemical conditions during dehydration (T and f/r ratios), heterogeneities in type, composition, and alteration of subducting lithologies. For example, Staudigel et al. (2010) speculated that volcanoclastic sediments, providing the greatest share of K as sedimentary input to the Mariana subduction zone, should be particularly predominant close to large seamounts; following the arguments in Mottl et al. (2004), it is very likely that K will be released from the slab, especially from volcanic turbidites, presumably even at T lower than those in our models. The average composition of subducting sediments used as input in our models will not take account of such variations. In addition, we also did not consider interactions between the different lithologies in the subduction channel, e.g., between ultramafic material and OIB, which would have added further complexity. More dedicated modeling and possibly experimental work would be needed to better reflect those natural fluid–rock interactions.

The key observations are, however, that at shallow subduction conditions 1) the release of K-containing fluids from subducting sediments and from AOC as well as 2) the uptake of K_2O by OIB, i.e., K_2O -metasomatism, are thermodynamically plausible, and 3) that this may lead to the formation of substantial amounts of phengite or other K-bearing phases. The models, in addition, imply K and other solutes such as Si, Ca, and Na to be elevated in slab-derived fluids at convergence margins across a range of thermal conditions, i.e., at both cool and warm subduction settings. The results hence strongly support the feasibility of metasomatic changes of (mafic) materials to occur in subduction channels at depths $\ll 30$ km.

Implications of Shallow Metasomatism and the Role of Phengite in Element Cycling

Following the results from this study and from the research conducted at the Mariana forearc over several decades, it has become clear that incoming lithologies must considerably change their composition at forearc depths. Independent of uncertainties in peak metamorphic conditions, this shallow transfer and redistribution of mass potentially has profound implications

for processes at deeper subduction levels. The shallow removal of certain elements from the subducting lithosphere affects the compositions of rocks that are subducted to beyond-forearc depths. Likewise, the mobilized elements impact fluid–rock reactions in the subduction channel and the mantle wedge. Low- to intermediate-grade metamorphic/metasomatic phases formed here, such as lawsonite and phengite (**Figures 5, 6**), will transport H_2O and elements to greater depths. Both minerals have extensive stability fields up to depths of >200 km (e.g., Poli and Schmidt, 1995; Schmidt, 1996). Phengite contains about 4 wt % H_2O and 12 wt% K_2O and is considered as an important carrier for these to and beyond sub-arc depths.

It is hence questionable whether K_2O and H_2O captured in phengite will ultimately be available to contribute to arc magmatism (also see discussion on phengite breakdown in, e.g., Chen et al., 2018). Our study demonstrates that the amount of phengite in individual metamafic rock clasts can (theoretically) be quite large. It cannot, however, be estimated how much phengite overall is being formed during such processes in other subduction systems. But seamounts depict substantial topographic irregularities on subducting oceanic plates and contribute to relief within the subduction channel, and it is well recognized that seamounts on outer-trench rises are deformed by faulting as the plate bends prior to subduction (e.g., Fryer and Smoot, 1985; Zhou and Lin, 2018). Subducting seamounts are subject to local increases in fluid pore pressure as they move through the subduction channel (e.g., Bell et al., 2010) and thus are prone to (further) deformation and possible decapitation (Watts et al., 2010). Although the detailed fate of deformation remains unclear (e.g., Wang and Bilek, 2014), it appears likely that much eroded material from subducted seamounts will be available for fluid–rock reactions (and fluid-induced metasomatism) in subduction channels/mélanges. With subduction channel thicknesses typically ranging from hundreds of meters to several kilometers (e.g., Cloos and Shreve, 1988; Guillot et al., 2009; Vannucchi et al., 2012) and the vast number of (eventually subducting) seamounts worldwide, it becomes clear that large masses of rock are likely to be compositionally (and mineralogically) modified. Bearing in mind the wide stability field of phengite (**Figure 5B**), we suppose that phengite formation in metamafics is potentially widespread throughout both cold and warm subduction zones.

Aside from being one of the major hosts for K in subduction environments, phengite is also known to incorporate high contents of fluid-mobile trace elements (e.g., Busigny et al., 2003; Bebout et al., 2013; Sievers et al., 2016). Studies on high- P minerals in eclogitic rocks from the Central Alps have shown that phengite can accommodate $>90\%$ of the whole-rock budget of Rb, Cs, and Ba (Zack et al., 2001). Determining the trace elemental distribution within the recycled OIBs is beyond the scope of this study, but bulk rock data imply enrichments in Rb, Cs, and to a lesser degree Th, as well as markedly lower Sr and Ba contents when compared to un-subducted Pacific seamounts (**Figure 8**). The losses in Sr and Ba can be explained by the breakdown of Ca plagioclase and/or of clays during the subduction of the OIB (e.g., Alt and Teagle, 2003; Putnis and John, 2010). Gains in Rb and Cs can putatively—as those in K_2O

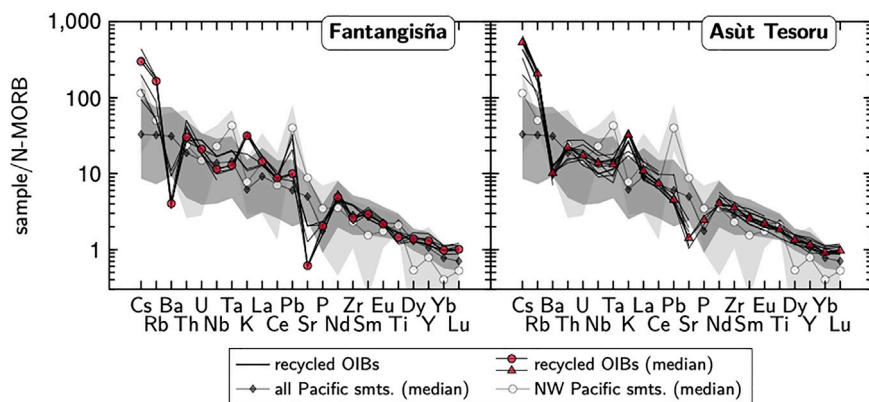


FIGURE 8 | Multi-element diagram for the recycled OIBs from Fantangisña and Asút Tesoru Seamounts normalized to N-type mid-ocean ridge basalt (Sun and McDonough, 1989). Data for the recycled OIBs are from Fryer et al. (2018); Fryer et al. (2020) and Deng et al. (2021). Values of K, P, and Ti are calculated from wt% oxide. Compositions of Pacific seamounts are shown for comparison (the dark gray and light gray fields represent the ranges in composition of all Pacific seamounts and NW Pacific seamounts, respectively, without the upper and lower 12.5% to account for outliers; note that <20 analyses are available for the NW Pacific seamounts except for K with $n = 67$ and Ti with $n = 62$, and that no Ba analyses are available; see *Methods* for more information and data sources).

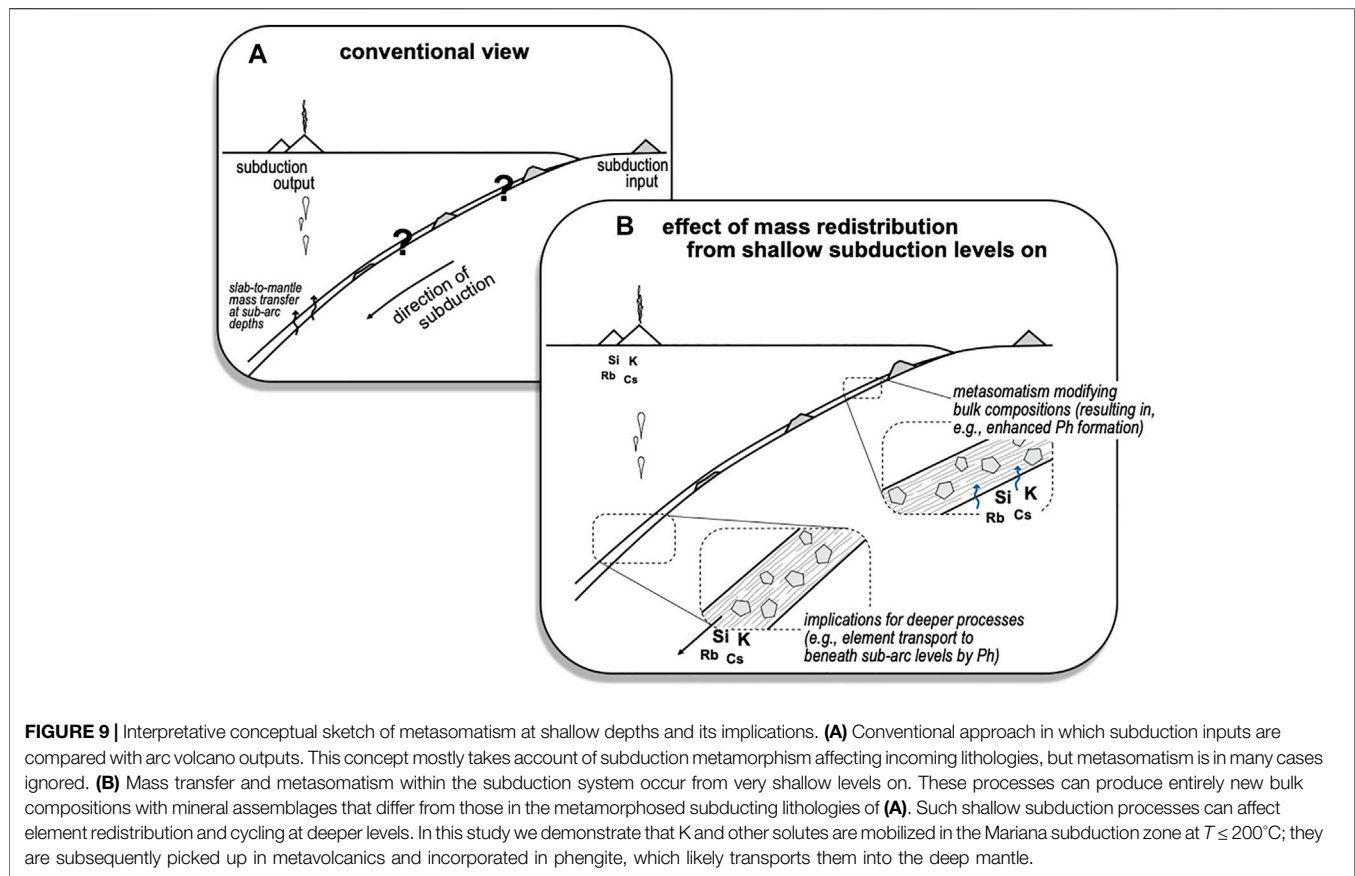
and SiO_2 —be ascribed to metasomatism in the subduction channel. Indeed, previous studies have shown that these elements are mobilized in the Mariana forearc and concentrations in the slab-fluids are high (e.g., Wheat et al., 2018; Albers et al., 2020). We speculate that much of the Rb and Cs is hosted by phengite. This interpretation is in accordance with considerably higher amounts of Rb and Cs at Asút Tesoru, relative to Fantangisña Seamount, from which phengite has primarily been reported (Ichiyama et al., 2021). Similarly, phengite in blueschist clasts from the South Chamorro Seamount, which has a similar depth-to-slab as Asút Tesoru, has been shown to be the major carrier of slab-released fluid-mobile elements (B, Li, and Be; Pabst et al., 2012). The observed fluid-metasomatism, resulting in enhanced phengite formation, thus also directly influences trace element budgets.

Would such an increased formation of phengite have a bearing on the importance of phlogopite, the K–Mg mica that was suggested to play a major role in the cycling of K_2O and H_2O ? Phlogopite crystallizes in the mantle wedge as a consequence of the infiltration of K-enriched slab-derived fluids, and it decomposes at deeper levels where it releases H_2O that in turn triggers mantle wedge partial melting and hence contributes to back-arc magmatism (e.g., Peacock, 1990; Sudo and Tatsumi, 1990). The phlogopite breakdown reactions also release K_2O , generating K-rich magmas (e.g., Foley & Peccerillo, 1992; Condamine and Médard, 2014). However, in the Izu–Bonin back-arc, Tamura et al. (2007) suggested that it is the breakdown of phengite that causes an increased mobility of K and consequently K-rich magmatism—whereas they attributed the scarcity of K-rich magmas in the arc-front to the presence and stability of phengite in the slab. And also other authors pointed out that phlogopite is not needed to generate K-rich melts (e.g., Wang et al., 2017). Our study highlights the complexity of the subduction channel’s mineralogy, which cannot be precisely defined. Potassium that is incorporated into phengite at shallow depths will unlikely be available to infiltrate the mantle wedge (to form phlogopite) somewhat deeper in the

system. It remains unclear how much of the slab-released K is trapped in the subduction channel and how much of it can rise into/through the mantle wedge. Yet, at least at the forearc of the Mariana subduction zone, K-enriched fluids expelled at the serpentinite mud volcanoes provide evidence that the amount of K released from the slab outweighs that incorporated at depths. The formation of phlogopite deeper within the Mariana subduction system hence appears plausible. Indeed, incompatible trace element abundances and isotopic compositions of primitive magmas from the Mariana arc imply the presence of phlogopite in the source region (e.g., Tamura et al., 2014).

Conclusively, our geochemical data and thermodynamic models imply that elements are mobilized and redistributed soon after the subduction of sediments and AOC at the Mariana convergent margin. This redistribution of mass from phases that are only stable at low P/T into metamorphic/metamorphic minerals such as phengite and/or lawsonite, both stable until great depths, will affect geochemical cycling of major and trace elements deep within subduction zones. We have conceptualized these processes in **Figure 9**.

In the literature, contrasting reports persist on the degree of element mobility in shallow subduction settings. For example, Bebout and Barton (1993) reported on blueschist metabasaltic rocks from the Catalina Schist (Catalina Island, CA) that exhibit K_2O enrichments up to >4 wt%, accompanied by enrichments of Cs and Ba. Sievers et al. (2016) provided evidence for the replacement of plagioclase by phengite in metadiorites and metagabbros, also from the Catalina Schist, and corresponding enrichments in K_2O and fluid-mobile trace elements. However, occurrences of exhumed blueschists (and also eclogites) with strongly elevated K_2O contents are rare. This is surprising considering that large amounts of K subduct as clays in pelagic sediment and AOC and the tendency of K to be released into the fluid phase at shallow subduction conditions (see, e.g., discussion in Kastner et al., 2014), i.e., the principal availability of K to interact with materials in the subduction



channel. Despite that, Shervais et al. (2011) documented prehnite–pumpellyite facies metavolcanics in a serpentinite mélange (Tehama–Colusa mélange, Coast Ranges, CA) that are enriched in SiO_2 and Na_2O , but not K_2O . Ghatak et al. (2012) even demonstrated that metamafic rocks that experienced up to eclogite metamorphism (Feather River ultramafic belt, Coast Ranges, CA) largely preserved their protolith major and trace elemental compositions except for some fluid-mobile elements such as Ba, Pb, and to a smaller extent La, U, and Sr. More generally, Harlov and Austrheim (2013) summarized that subducting sediments and probably also igneous crustal rocks can largely retain their inventories of even the more fluid-mobile elements to at least 90 km in relatively cool subduction zones; higher geothermal gradients may generate greater forearc devolatilization leading to greater loss of fluids and fluid-mobile elements to the mantle wedge. They further stated that, at forearc depths, only the extremely mobile elements (for instance B, Cs, As, and Sb for the blueschist metasedimentary suite of the Catalina Schist) show a clear record of whole-rock loss, as based on comparisons between higher-grade rocks with lower-grade or unmetamorphosed equivalents.

A number of factors may influence the liberation of elements as well as metasomatic processes occurring soon after subduction, including the composition and state of the incoming lithosphere (i.e., type and thickness of sediment, nature and degree of alteration of the oceanic basement) and the thermal structure of the system. The variety of these in subduction zones worldwide

likely leads to decreased element mobility in some and elevated mobility in other sites. Further, the position of subducting rock within the convergent margin—it could metamorphose/metamorphose as part of the intact volcanic basement, could be positioned in the vicinity of a fluid conduit, or float within the subduction channel—is an important additional factor that contributes to the variability of element mobility (see discussion and references in Spandler and Pirard, 2013). Within the intact basement, rocks potentially mostly dehydrate at low f/r ratios and are being depleted in fluid-mobile elements (that are, once released, transported towards the upper plate). Since the subducting lithosphere provides a vast reservoir, large amounts of fluids and elements will be mobilized even though the elemental losses in individual portions of rock may appear minor and imply subduction metamorphism in a (more or less) closed system. Rocks situated along fluid pathways or in the subduction channel mélange, however, interact with slab-fluids at higher f/r ratios, leading to more increased modifications.

In the Mariana forearc, the extensive fluid–rock reactions in the subduction channel are particularly well documented. Enrichments (or depletions) of certain elements in rock clasts (this study; see also, e.g., Johnson, et al., 2014; Kahl et al., 2015; Tamblyn et al., 2019; Albers et al., 2020) allowed reconstructing processes in the subducting slab and during the fluids' rise toward the forearc seafloor. Serpentinites, for instance, incorporate fluid-mobile elements (Wei et al., 2006; Savov et al., 2007; Debret et al., 2019). Yet, despite high concentrations of these in the rocks,

fluids emanating at the mud volcano summits still are considerably enriched in the same elements, implying that the mobilized amounts of these exceed what serpentinites can take up. Considering the putatively vast volumes of serpentinite produced in the Mariana forearc (e.g., Cai et al., 2018), the amount of mass mobilized from the slab must be immense. Research at the serpentinite mud volcanoes has clearly pointed out the significance of the liberation and transfer of fluids and mass at subduction depths <30 km. In line with these results, Kastner et al. (2014) estimated the global return flux of fluids and solutes from forearcs to the ocean through seeps and fault-controlled conduits to be large enough to importantly impact seawater chemistry (such as Mg, Ca, or SO₄).

Mass transfer and associated metasomatic processes that set in at shallow forearc depths are, however, often overlooked when geochemical cycling in subduction zones is investigated. Many (modeling) studies compare subduction inputs to arc volcanic outputs without considering metasomatism-related phase transitions. Our results strongly suggest that, for a holistic view, these processes need to be integrated. In line with these implications, previous studies concluded that up to kilometer-thick mélangé zones in the subduction channel (formed during the mechanical mixing of materials from the subducting and overriding plates) may ultimately control the nature and composition of slab-derived fluids that enter the mantle wedge (e.g., King et al., 2006; Marschall and Schumacher, 2012; see also; Spandler and Pirard, 2013).

SUMMARY AND CONCLUSIONS

Data and models presented here provide unique insight regarding fluid-induced mass transfer and metasomatism within the shallow depths of an active subduction zone. We demonstrate that subducted OIB clasts have undergone substantial compositional changes, most likely at conditions that did not largely exceed 7–8 kbar and 200–350°C. Most noticeable and consistent throughout all clasts are enrichments in K₂O and H₂O, accompanied by SiO₂, Na₂O, and MgO gains in samples from Fantangisña Seamount and SiO₂ gains but MgO and Fe₂O₃* losses in samples from Asút Tesoru Seamount. In addition, the fluid-mobile elements Cs and Rb are increased whereas Ba and Sr contents are decreased in all samples.

The metasomatic changes can be explained by the interaction of element-laden, slab-derived fluids with (fragmented) parts of subducted seamounts in the subduction channel. Our reaction path models predict the release of fluids enriched in K and other solutes from subducting oceanic lithosphere even at $T < 200^{\circ}\text{C}$, consistent with known compositions of slab-derived fluids at the Mariana forearc seafloor. A K₂O-increase in OIB during its reaction with the above fluid is thermodynamically feasible.

The observed changes in major element composition have considerable ramifications for the clasts' metamorphic phase assemblages. Our equilibrium assemblage diagrams predict a strikingly increased stability field and much greater absolute amounts of phengite (up to four times as much) relative to unmetasomatized OIB. Phengite in turn can carry K₂O, H₂O, and fluid-mobile trace elements beyond sub-arc depths.

These results highlight the importance of acknowledging subduction processes at shallow depths (<30 km) as they may play a fundamental role in controlling *which* components as well as *in which state* (i.e., bound in which minerals) these components ultimately reach greater depths where they may or may not contribute to arc magmatism. We suggest that metasomatic/rock transformation processes likely take place shallow within all subduction zones, and that these processes could affect all subducted rock types including sediments, MORB, and OIB as well as the base of the mantle wedge.

DATA AVAILABILITY STATEMENT

The original contributions presented in the study are included in the article/**Supplementary Material**, further inquiries can be directed to the corresponding author.

AUTHOR CONTRIBUTIONS

EA, JWS, YI, and PF sailed IODP Exp. 366. EA planned and designed the study. YI and EA examined the samples petrologically; bulk rock analyses were conducted by JWS. EA performed thermodynamic calculations; CTH and EA compiled the thermodynamic database for EQ3/6. The manuscript was written by EA with contributions of all co-authors.

FUNDING

EA acknowledges funding by the Special Priority Program 527 “International Ocean Discovery Program” of the German Research Foundation (DFG), grant BA 1605/18–1, and by the Helmholtz Association “POSY – The Polar System and its Effects on the Ocean Floor” (project no. ExNet-0001-Phase2-3). PF acknowledges funding by IODP-US Science Support Program. This is publication SOEST #11477/HIGP#2458.

ACKNOWLEDGMENTS

This research used samples and data provided by IODP. We are grateful to the captain and crew of the D/V JOIDES Resolution, to the IODP science technicians, and to the Exp. 366 Science Party. We greatly appreciate editorial handling by Philipp A. Brandl and constructive reviews by Jeffrey Alt and Xu Chu. The processing charges for this open-access article were covered by the University of Bremen. A preprint of this article has been uploaded to EarthArXiv and is available at <https://doi.org/10.31223/x56d1s>.

SUPPLEMENTARY MATERIAL

The Supplementary Material for this article can be found online at: <https://www.frontiersin.org/articles/10.3389/feart.2022.826312/full#supplementary-material>

REFERENCES

- Albers, E., Bach, W., Klein, F., Menzies, C. D., Lucassen, F., and Teagle, D. A. H. (2019). Fluid-rock Interactions in the Shallow Mariana Forearc: Carbon Cycling and Redox Conditions. *Solid Earth* 10, 907–930. doi:10.5194/se-10-907-2019
- Albers, E., Kahl, W.-A., Beyer, L., and Bach, W. (2020). Variant Across-Forearc Compositions of Slab-Fluids Recorded by Serpentinites: Implications on the Mobilization of FMEs from an Active Subduction Zone (Mariana Forearc). *Lithos* 364–365, 105525. doi:10.1016/j.lithos.2020.105525
- Alt, J. C. (1995). Subseafloor Processes in Mid-ocean Ridge Hydrothermal Systems. *Geophys. Monogr. Ser.* 91, 85–114. doi:10.1029/gm091p0085
- Alt, J. C., and Teagle, D. A. H. (2003). Hydrothermal Alteration of Upper Oceanic Crust Formed at a Fast-Spreading Ridge: Mineral, Chemical, and Isotopic Evidence from ODP Site 801. *Chem. Geol.* 201, 191–211. doi:10.1016/S0009-2541(03)00201-8
- Bach, W., Jöns, N., and Klein, F. (2013). “Metasomatism within the Ocean Crust,” in *Metasomatism and the Chemical Transformation of Rock, Lecture Notes in Earth System Sciences*. Editors D. E. Harlov and H. Austrheim (Berlin, Heidelberg: Springer), 253–288. doi:10.1007/978-3-642-28394-9_8
- Baker, P. E., Castillo, P. R., and Condliffe, E. (1995). “Petrology and Geochemistry of Igneous Rocks from Allison and Resolution Guyots, Sites 865 and 866,” in *Proc. ODP, Sci. Results*. Editors E. L. Winterer, W. W. Sager, J. V. Firth, and J. M. Sinton (College Station, TX: Ocean Drilling Program), 143, 245–261. doi:10.2973/odp.proc.sr.143.216.1995
- Baldwin, J. A., Powell, R., Brown, M., Moraes, R., and Fuck, R. A. (2005). Modelling of mineral Equilibria in Ultrahigh-Temperature Metamorphic Rocks from the Anápolis-Itaçu Complex, central Brazil. *J. Metamorph. Geol.* 23, 511–531. doi:10.1111/j.1525-1314.2005.00591.x
- Bebout, G. E., Agard, P., Kobayashi, K., Moriguti, T., and Nakamura, E. (2013). Devolatilization History and Trace Element Mobility in Deeply Subducted Sedimentary Rocks: Evidence from Western Alps HP/UHP Suites. *Chem. Geol.* 342, 1–20. doi:10.1016/j.chemgeo.2013.01.009
- Bebout, G. E., and Barton, M. D. (1993). Metasomatism during Subduction: Products and Possible Paths in the Catalina Schist, California. *Chem. Geol.* 108, 61–92. doi:10.1016/0009-2541(93)90318-d
- Bebout, G. E., Ryan, J. G., Leeman, W. P., and Bebout, A. E. (1999). Fractionation of Trace Elements by Subduction-Zone Metamorphism - Effect of Convergent-Margin thermal Evolution. *Earth Planet. Sci. Lett.* 171, 63–81. doi:10.1016/s0012-821x(99)00135-1
- Bekins, B., McCaffrey, A. M., and Dreiss, S. J. (1994). Influence of Kinetics on the Smectite to Illite Transition in the Barbados Accretionary Prism. *J. Geophys. Res.* 99, 18147–18158. doi:10.1029/94jb01187
- Bell, R., Sutherland, R., Barker, D. H. N., Henrys, S., Bannister, S., Wallace, L., et al. (2010). Seismic Reflection Character of the Hikurangi Subduction Interface, New Zealand, in the Region of Repeated Gisborne Slow Slip Events. *Geophys. J. Int.* 180, 34–48. doi:10.1111/j.1365-246x.2009.04401.x
- Busigny, V., Cartigny, P., Philippot, P., Ader, M., and Javoy, M. (2003). Massive Recycling of Nitrogen and Other Fluid-mobile Elements (K, Rb, Cs, H) in a Cold Slab Environment: Evidence from HP to UHP Oceanic Metasediments of the Schistes Lustrés Nappe (Western Alps, Europe). *Earth Planet. Sci. Lett.* 215, 27–42. doi:10.1016/s0012-821x(03)00453-9
- Cai, C., Wiens, D. A., Shen, W., and Eimer, M. (2018). Water Input into the Mariana Subduction Zone Estimated from Ocean-Bottom Seismic Data. *Nature* 563, 389–392. doi:10.1038/s41586-018-0655-4
- Chen, S., Guo, X., Yoshino, T., Jin, Z., and Li, P. (2018). Dehydration of Phengite Inferred by Electrical Conductivity Measurements: Implication for the High Conductivity Anomalies Relevant to the Subduction Zones. *Geology* 46, 11–14. doi:10.1130/g39716.1
- Cloos, M., and Shreve, R. L. (1988). Subduction-channel Model of Prism Accretion, Melange Formation, Sediment Subduction, and Subduction Erosion at Convergent Plate Margins: 1. Background and Description. *Pageoph* 128, 455–500. doi:10.1007/bf00874548
- Codillo, E. A., Le Roux, V., and Marschall, H. R. (2018). Arc-like Magmas Generated by Mélange-Peridotite Interaction in the Mantle Wedge. *Nat. Commun.* 9, 2864. doi:10.1038/s41467-018-05313-2
- Condamine, P., and Médard, E. (2014). Experimental Melting of Phlogopite-Bearing Mantle at 1 GPa: Implications for Potassic Magmatism. *Earth Planet. Sci. Lett.* 397, 80–92. doi:10.1016/j.epsl.2014.04.027
- Davis, A. S., Pringle, M. S., Pickthorn, L.-B. G., Clague, D. A., and Schwab, W. C. (1989). Petrology and Age of Alkalic Lava from the Ratak Chain of the Marshall Islands. *J. Geophys. Res.* 94, 5757–5774. doi:10.1029/jb094ib05p05757
- de Capitani, C., and Brown, T. H. (1987). The Computation of Chemical Equilibrium in Complex Systems Containing Non-ideal Solutions. *Geochim. Cosmochim. Acta* 51, 2639–2652. doi:10.1016/0016-7037(87)90145-1
- de Capitani, C., and Petrakakis, K. (2010). The Computation of Equilibrium Assemblage Diagrams with Theriak/Domino Software. *Am. Mineral.* 95, 1006–1016. doi:10.2138/am.2010.3354
- Debret, B., Albers, E., Walter, B., Price, R., Barnes, J. D., Beunon, H., et al. (2019). Shallow Forearc Mantle Dynamics and Geochemistry: New Insights from IODP Expedition 366. *Lithos* 326–327, 230–245. doi:10.1016/j.lithos.2018.10.038
- Deng, J., Zhang, L., Liu, H., Liu, H., Liao, R., Mastoi, A. S., et al. (2021). Geochemistry of Subducted Metabasites Exhumed from the Mariana Forearc: Implications for Pacific Seamount Subduction. *Geosci. Front.* 12, 101117. doi:10.1016/j.gsf.2020.12.002
- Deschamps, F., Guillot, S., Godard, M., Andreani, M., and Hattori, K. (2011). Serpentinites Act as Sponges for Fluid-mobile Elements in Abyssal and Subduction Zone Environments. *Terra Nova* 23, 171–178. doi:10.1111/j.1365-3121.2011.00995.x
- Ernst, W. G. (1984). Californian Blueschists, Subduction, and the Significance of Tectonostratigraphic Terranes. *Geology* 12, 436–440. doi:10.1130/0091-7613(1984)12<436:cbats>2.0.co;2
- Foley, S., and Peccerillo, A. (1992). Potassic and Ultrapotassic Magmas and Their Origin. *Lithos* 28, 181–185. doi:10.1016/0024-4937(92)90005-j
- Fryer, P., Ambos, E. L., and Hussong, D. M. (1985). Origin and Emplacement of Mariana Forearc Seamounts. *Geology* 13, 774–777. doi:10.1130/0091-7613(1985)13<774:oeomf>2.0.co;2
- Fryer, P., Gharib, J., Ross, K., Savov, I., and Mottl, M. J. (2006). Variability in Serpentine Mudflow Mechanisms and Sources: ODP Drilling Results on Mariana Forearc Seamounts. *Geochem. Geophys. Geosyst.* 7. doi:10.1029/2005gc001201
- Fryer, P., Mottl, M., Johnson, L., Haggerty, J., Phipps, S., and Maekawa, H. (1995). Serpentine Bodies in the Forearcs of Western Pacific Convergent Margins: Origin and Associated Fluids. *Geophys. Monogr. Ser.* 88, 259–279. doi:10.1029/gm088p0259
- Fryer, P., Pearce, J. A., Stokking, L. B., et al. (1992). *Proc. ODP, Sci. Results*, 125. College Station, TX: Ocean Drilling Program. doi:10.2973/odp.proc.sr.125.1992
- Fryer, P. (2012). Serpentine Mud Volcanism: Observations, Processes, and Implications. *Annu. Rev. Mar. Sci.* 4, 345–373. doi:10.1146/annurev-marine-120710-100922
- Fryer, P., and Smoot, N. C. (1985). Processes of Seamount Subduction in the Mariana and Izu-Bonin Trenches. *Mar. Geol.* 64, 77–90. doi:10.1016/0025-3227(85)90161-6
- Fryer, P., Wheat, C. G., Williams, T., Kelley, C., Johnson, K., Ryan, J., et al. (2020). Mariana Serpentine Mud Volcanism Exhumes Subducted Seamount Materials: Implications for the Origin of Life. *Phil. Trans. R. Soc. A.* 378, 20180425. doi:10.1098/rsta.2018.0425
- Fryer, P., Wheat, C., Williams, T., and The Expedition 366 Scientists (2018). “Mariana Convergent Margin and South Chamorro Seamount,” in *Proc. ODP, Init. Repts.* (College Station, TX: International Ocean Discovery Program), 366. doi:10.14379/iodep.proc.366.101.2018
- Geilert, S., Albers, E., Frick, D. A., Hansen, C. T., and von Blanckenburg, F. (2021). Systematic Changes in Serpentine Si Isotope Signatures across the Mariana Forearc - a New Proxy for Slab Dehydration Processes. *Earth Planet. Sci. Lett.* 575, 117193. doi:10.1016/j.epsl.2021.117193
- Geilert, S., Grasse, P., Wallmann, K., Liebetrau, V., and Menzies, C. D. (2020). Serpentine Alteration as Source of High Dissolved Silicon and Elevated $\delta^{30}\text{Si}$ Values to the marine Si Cycle. *Nat. Commun.* 11, 5123. doi:10.1038/s41467-020-18804-y
- Ghatak, A., Basu, A. R., and Wakabayashi, J. (2012). Elemental Mobility in Subduction Metamorphism: Insight from Metamorphic Rocks of the Franciscan Complex and the Feather River Ultramafic Belt, California. *Int. Geol. Rev.* 54, 654–685. doi:10.1080/00206814.2011.567087
- Giarmita, M., MacPherson, G. J., and Phipps, S. P. (1988). Petrologically Diverse Basalts from a Fossil Oceanic Forearc in California: the Llanada and Black

- Mountain Remnants of the Coast Range Ophiolite. *Geol. Soc. Am. Bull.* 110, 553–571. doi:10.1130/0016-7606(1998)110<0553:pdbfaf>2.3.co;2
- Grant, J. A. (1986). The Isocon Diagram; a Simple Solution to Gresens' Equation for Metasomatic Alteration. *Econ. Geol.* 81, 1976–1982. doi:10.2113/gsecongeo.81.8.1976
- Gresens, R. L. (1967). Composition-volume Relationships of Metasomatism. *Chem. Geol.* 2, 47–65. doi:10.1016/0009-2541(67)90004-6
- Guillot, S., Hattori, K., Agard, P., Schwarz, S., and Vidal, O. (2009). "Exhumation Processes in Oceanic and continental Subduction Contexts: a Review," in *Subduction Zone Geodynamics*. Editors S. Lallemand and F. Funicello (Berlin Heidelberg: Springer). doi:10.1007/978-3-540-87974-9
- Harlow, D. E., and Austrheim, H. (2013). *Metasomatism and the Chemical Transformation of Rock: The Role of Fluids in Terrestrial and Extraterrestrial Processes*. Berlin/Heidelberg: Springer. doi:10.1007/978-3-642-28394-9
- Holland, T. J. B., and Powell, R. (2011). An Improved and Extended Internally Consistent Thermodynamic Dataset for Phases of Petrological Interest, Involving a New Equation of State for Solids. *J. Metamorph. Geol.* 29, 333–383. doi:10.1111/j.1525-1314.2010.00923.x
- Holland, T. J. B., and Powell, R. (1998). An Internally Consistent Thermodynamic Data Set for Phases of Petrological Interest. *J. Metamorph. Geol.* 16, 309–343. doi:10.1111/j.1525-1314.1998.00140.x
- Holland, T., and Powell, R. (2003). Activity-composition Relations for Phases in Petrological Calculations: an Asymmetric Multicomponent Formulation. *Contrib. Mineral. Petrol.* 145, 492–501. doi:10.1007/s00410-003-0464-z
- Hulme, S. M., Wheat, C. G., Fryer, P., and Mottl, M. J. (2010). Pore Water Chemistry of the Mariana Serpentinite Mud Volcanoes: a Window to the Seismogenic Zone. *Geochem. Geophys. Geosyst.* 11. doi:10.1029/2009gc002674
- Ichiyama, Y., Tsujimori, T., Fryer, P., Michibayashi, K., Tamura, A., and Morishita, T. (2021). Temporal and Spatial Mineralogical Changes in Clasts from Mariana Serpentinite Mud Volcanoes: Cooling of the Hot Forearc-Mantle at Subduction Initiation. *Lithos* 384–385, 105941. doi:10.1016/j.lithos.2020.105941
- Jackson, M. G., and Dasgupta, R. (2008). Compositions of HIMU, EM1, and EM2 from Global Trends between Radiogenic Isotopes and Major Elements in Ocean Island Basalts. *Earth Planet. Sci. Lett.* 276, 175–186. doi:10.1016/j.epsl.2008.09.2310.1016/j.epsl.2008.09.023
- Janney, P. E., and Castillo, P. R. (1999). Isotope Geochemistry of the Darwin Rise Seamounts and the Nature of Long-Term Mantle Dynamics beneath the South central Pacific. *J. Geophys. Res.* 104, 10571–10589. doi:10.1029/1998jb900061
- Jayko, A. S., Blake, M. C., and Brothers, R. N. (1986). Blueschist Metamorphism of the Eastern Franciscan Belt, Northern California. *Geol. Soc. Am. Mem.* 164, 107–124. doi:10.1130/mem164-p107
- Johnson, J. A., Hickey-Vargas, R., Fryer, P., Salters, V., and Reagan, M. K. (2014). Geochemical and Isotopic Study of a Plutonic Suite and Related Early Volcanic Sequences in the Southern Mariana Forearc. *Geochem. Geophys. Geosyst.* 15, 589–604. doi:10.1002/2013gc005053
- Kahl, W.-A., Jöns, N., Bach, W., Klein, F., and Alt, J. C. (2015). Ultramafic Clasts from the South Chamorro Serpentine Mud Volcano Reveal a Polyphase Serpentinization History of the Mariana Forearc Mantle. *Lithos* 227, 1–20. doi:10.1016/j.lithos.2015.03.015
- Kastner, M., Solomon, E. A., Harris, R. N., and Torres, M. E. (2014). "Fluid Origins, thermal Regimes, and Fluid and Solute Fluxes in the Forearc of Subduction Zones," in *Earth and Life Processes Discovered from Seafloor Environments: A Decade of Science Achieved by the Integrated Ocean Drilling Program (IODP)*. Editors R. Stein, D. K. Blackman, F. Inagaki, and H.-C. Larsen (Amsterdam, Netherlands: Elsevier), 7, 671–733. doi:10.1016/b978-0-444-62617-2.00022-0
- Kelley, K. A., Plank, T., Ludden, J., and Staudigel, H. (2003). Composition of Altered Oceanic Crust at ODP Sites 801 and 1149. *Geochem. Geophys. Geosyst.* 4. doi:10.1029/2002gc000435
- King, R., Bebout, G., Moriguti, T., and Nakamura, E. (2006). Elemental Mixing Systematics and Sr-Nd Isotope Geochemistry of Mélange Formation: Obstacles to Identification of Fluid Sources to Arc Volcanics. *Earth Planet. Sci. Lett.* 246, 288–304. doi:10.1016/j.epsl.2006.03.053
- Koppers, A. A. P., Staudigel, H., Wijbrans, J. R., and Pringle, M. S. (1998). The Magellan Seamount Trail: Implications for Cretaceous Hotspot Volcanism and Absolute Pacific Plate Motion. *Earth Planet. Sci. Lett.* 163, 53–68. doi:10.1016/s0012-821x(98)00175-7
- Leat, P. T., and Larter, R. D. (2003). Intra-oceanic Subduction Systems: Introduction. *Geol. Soc. Lond. Spec. Publ.* 219, 1–17. doi:10.1144/gsl.sp.2003.219.01.01
- Liu, Y., Zhang, G., Zhang, J., and Wang, S. (2020). Geochemical Constraints on CO₂-rich Mantle Source for the Kocebu Seamount, Magellan Seamount Chain in the Western Pacific. *J. Ocean. Limnol.* 38, 1201–1214. doi:10.1007/s00343-020-0013-x
- Lockwood, J. P. (1972). Possible Mechanisms for the Emplacement of alpine-type Serpentinite. *Geol. Soc. Am. Mem.* 132, 273–288. doi:10.1130/mem132-p273
- Maekawa, H., Shozul, M., Ishll, T., Fryer, P., and Pearce, J. A. (1993). Blueschist Metamorphism in an Active Subduction Zone. *Nature* 364, 520–523. doi:10.1038/364520a0
- Manning, C. (2004). The Chemistry of Subduction-Zone Fluids. *Earth Planet. Sci. Lett.* 223, 1–16. doi:10.1016/j.epsl.2004.04.030
- Marschall, H. R., and Schumacher, J. C. (2012). Arc Magmas Sourced from Mélange Diapirs in Subduction Zones. *Nat. Geosci.* 5, 862–867. doi:10.1038/ngeo1634
- Menzies, C. D., Price, R. E., Ryan, J., Sissmann, O., Takai, K., and Wheat, C. G. (2022). Spatial Variation of Subduction Zone Fluids during Progressive Subduction: Insights from Serpentinite Mud Volcanoes. *Geochim. Cosmochim. Acta* 319, 118–134. doi:10.1016/j.gca.2021.10.030
- Moore, J. C., and Vrolijk, P. (1992). Fluids in Accretionary Prisms. *Rev. Geophys.* 30, 113–135. doi:10.1029/92rg00201
- Mottl, M. J., Wheat, C. G., Fryer, P., Gharib, J., and Martin, J. B. (2004). Chemistry of Springs across the Mariana Forearc Shows Progressive Devolatilization of the Subducting Plate. *Geochim. Cosmochim. Acta* 68, 4915–4933. doi:10.1016/j.gca.2004.05.037
- Oakley, A. J. (2008). A Multi-Channel Seismic and Bathymetric Investigation of the central Mariana Convergent Margin. PhD Thesis. Manoa, HI: University of Hawai'i.
- Oakley, A. J., Taylor, B., and Moore, G. F. (2008). Pacific Plate Subduction beneath the central Mariana and Izu-Bonin Fore Arcs: New Insights from an Old Margin. *Geochem. Geophys. Geosyst.* 9. doi:10.1029/2007gc001820
- Pabst, S., Zack, T., Savov, I. P., Ludwig, T., Rost, D., Tonarini, S., et al. (2012). The Fate of Subducted Oceanic Slabs in the Shallow Mantle: Insights from Boron Isotopes and Light Element Composition of Metasomatized Blueschists from the Mariana Forearc. *Lithos* 132–133, 162–179. doi:10.1016/j.lithos.2011.11.010
- Pattison, D. R. M., De Capitani, C., and Gaidies, F. (2011). Petrological Consequences of Variations in Metamorphic Reaction Affinity. *J. Metamorph. Geol.* 29, 953–977. doi:10.1111/j.1525-1314.2011.00950.x
- Peacock, S. A. (1990). Fluid Processes in Subduction Zones. *Science* 248, 329–337. doi:10.1126/science.248.4953.329
- Peacock, S. M., and Wang, K. (1999). Seismic Consequences of Warm versus Cool Subduction Metamorphism: Examples from Southwest and Northeast Japan. *Science* 286, 937–939. doi:10.1126/science.286.5441.937
- Perfit, M. R., Gust, D. A., Bence, A. E., Arculus, R. J., and Taylor, S. R. (1980). Chemical Characteristics of Island-Arc Basalts: Implications for Mantle Sources. *Chem. Geol.* 30, 227–256. doi:10.1016/0009-2541(80)90107-2
- Plank, T., and Langmuir, C. H. (1998). The Chemical Composition of Subducting Sediment and its Consequences for the Crust and Mantle. *Chem. Geol.* 145, 325–394. doi:10.1016/s0009-2541(97)00150-2
- Plank, T., Ludden, J. N., Escutia, C., et al. (2000). *Proc. ODP, Init. Repts.*. TX: Ocean Drilling Program, 185. doi:10.2973/odp.proc.ir.185.2000
- Poli, S., and Schmidt, M. W. (1995). H₂O Transport and Release in Subduction Zones: Experimental Constraints on Basaltic and Andesitic Systems. *J. Geophys. Res.* 100, 22299–22314. doi:10.1029/95jb01570
- Pons, M.-L., Quitte, G., Fujii, T., Rosing, M. T., Reynard, B., Moynier, F., et al. (2011). Early Archean Serpentine Mud Volcanoes at Isua, Greenland, as a Niche for Early Life. *Proc. Natl. Acad. Sci.* 108, 17639–17643. doi:10.1073/pnas.1108061108
- Putnis, A., and Austrheim, H. (2010). Fluid-induced Processes: Metasomatism and Metamorphism. *Geofluids* 10, 254–269. doi:10.1111/j.1468-8123.2010.00285.x
- Putnis, A., and John, T. (2010). Replacement Processes in the Earth's Crust. *Elements* 6, 159–164. doi:10.2113/gselements.6.3.159
- Ringwood, A. E. (1969). Composition and Evolution of the Upper Mantle. *Geoph. Monog. Ser.* 13, 1–17. doi:10.1029/gm013p0001
- Rustioni, G., Audetat, A., and Keppler, H. (2021). The Composition of Subduction Zone Fluids and the Origin of the Trace Element Enrichment in Arc Magmas. *Contrib. Mineral. Petrol.* 176, 51. doi:10.1007/s00410-021-01810-8
- Savov, I. P., Guggino, S., Ryan, J. G., Fryer, P., and Mottl, M. J. (2005a). "Geochemistry of Serpentinite Muds and Metamorphic Rocks from the

- Mariana Forearc, ODP Sites 1200 and 778-779, South Chamorro and Conical Seamounts," in *Proc. ODP, Sci. Results*. Editors M. Shinohara, M. H. Salisbury, and C. Richter (College Station, TX: Ocean Drilling Program), 195, 1-49. doi:10.2973/odp.proc.sr.195.103.2005
- Savov, I. P., Ryan, J. G., D'Antonio, M., Kelley, K., and Mattie, P. (2005b). Geochemistry of Serpentinized Peridotites from the Mariana Forearc Conical Seamount, ODP Leg 125: Implications for the Elemental Recycling at Subduction Zones. *Geochem. Geophys. Geosyst.* 6. doi:10.1029/2004gc000777
- Savov, I. P., Ryan, J. G., D'Antonio, M., and Fryer, P. (2007). Shallow Slab Fluid Release across and along the Mariana Arc-basin System: Insights from Geochemistry of Serpentinized Peridotites from the Mariana Fore Arc. *J. Geophys. Res.* 112, B09205. doi:10.1029/2006jb004749
- Scambelluri, M., and Philippot, P. (2001). Deep Fluids in Subduction Zones. *Lithos* 55, 213-227. doi:10.1016/s0024-4937(00)00046-3
- Schmidt, M. W. (1996). Experimental Constraints on Recycling of Potassium from Subducted Oceanic Crust. *Science* 272, 1927-1930. doi:10.1126/science.272.5270.1927
- Shervais, J. W., Choi, S. H., Sharp, W. D., Ross, J., Zogman-Schuman, M., and Mukasa, S. B. (2011). Serpentinite Matrix Mélange: Implications of Mixed Provenance for Mélange Formation. *Geol. Soc. Am. Spec. Pap.* 480, 1-38. doi:10.1130/2011.2480(01)10.1130/2011.2480(01)
- Shervais, J. W., Reagan, M., Haugen, E., Almeev, R. R., Pearce, J. A., Prytulak, J., et al. (2019). Magmatic Response to Subduction Initiation: Part 1. Fore-arc Basalts of the Izu-Bonin Arc from IODP Expedition 352. *Geochem. Geophys. Geosyst.* 20, 314-338. doi:10.1029/2018gc007731
- Shervais, J. W. (2022). The Petrogenesis of Modern and Ophiolitic Lavas Reconsidered: Ti-V and Nb-Th. *Geosci. Front.* 13, 101319. doi:10.1016/j.gsf.2021.101319
- Shervais, J. W. (1982). Ti-V Plots and the Petrogenesis of Modern and Ophiolitic Lavas. *Earth Planet. Sci. Lett.* 59, 101-118. doi:10.1016/0012-821x(82)90120-0
- Sievers, N. E., Tenore, J., Penniston-Dorland, S. C., and Bebout, G. E. (2016). Fingerprints of Forearc Element Mobility in Blueschist-Facies Metaconglomerates, Catalina Schist, California. *Int. Geol. Rev.* 59, 741-752. doi:10.1080/00206814.2016.1253038
- Spandler, C., and Pirard, C. (2013). Element Recycling from Subducting Slabs to Arc Crust: a Review. *Lithos* 170-171, 208-223. doi:10.1016/j.lithos.2013.02.016
- Staudigel, H. (2014). "Chemical Fluxes from Hydrothermal Alteration of the Oceanic Crust," in *Treatise on Geochemistry* (Amsterdam, Netherlands: Elsevier), 583-606. doi:10.1016/b978-0-08-095975-7.00318-1
- Staudigel, H., Koppers, A., Plank, T., and Hanan, B. (2010). Seamounts in the Subduction Factory. *Oceanogr.* 23, 176-181. doi:10.5670/oceanog.2010.69
- Staudigel, H., Plank, T., White, B., and Schmincke, H.-U. (1996). Geochemical Fluxes during Seafloor Alteration of the Basaltic Upper Oceanic Crust: DSDP Sites 417 and 418. *Geoph. Monog. Ser.* 96, 19-38. doi:10.1029/gm096p0019
- Stern, R. J. (2002). Subduction Zones. *Rev. Geophys.* 40, 31012. doi:10.1029/2001rg000108
- Sudo, A., and Tatsumi, Y. (1990). Phlogopite and K-Amphibole in the Upper Mantle: Implication for Magma Genesis in Subduction Zones. *Geophys. Res. Lett.* 17, 29-32. doi:10.1029/gl017i001p00029
- Sun, S.-s., and McDonough, W. F. (1989). Chemical and Isotopic Systematics of Oceanic Basalts: Implications for Mantle Composition and Processes. *Geol. Soc. Lond. Spec. Publ.* 42, 313-345. doi:10.1144/gsl.sp.1989.042.01.19
- Tamblyn, R., Zack, T., Schmitt, A. K., Hand, M., Kelsey, D., Morrissey, L., et al. (2019). Blueschist from the Mariana Forearc Records Long-Lived Residence of Material in the Subduction Channel. *Earth Planet. Sci. Lett.* 519, 171-181. doi:10.1016/j.epsl.2019.05.013
- Tamura, Y., Ishizuka, O., Stern, R. J., Nichols, A. R. L., Kawabata, H., Hirahara, Y., et al. (2014). Mission Immiscible: Distinct Subduction Components Generate Two Primary Magmas at Pagan Volcano, Mariana Arc. *J. Petrol.* 55, 63-101. doi:10.1093/petrology/egt061
- Tamura, Y., Tani, K., Chang, Q., Shukuno, H., Kawabata, H., Ishizuka, O., et al. (2007). Wet and Dry Basalt Magma Evolution at Torishima Volcano, Izu-Bonin Arc, Japan: the Possible Role of Phengite in the Downgoing Slab. *J. Petrol.* 48, 1999-2031. doi:10.1093/petrology/egm048
- Tang, L., Dong, Y., Chu, F., Chen, L., Ma, W., and Liu, Y. (2019). Geochemistry and Age of Seamounts in the West Pacific: Mantle Processes and Petrogenetic Implications. *Acta Oceanol. Sin.* 38, 71-77. doi:10.1007/s13131-019-1371-0
- Tatsumi, Y., and Eggins, S. (1995). *Subduction Zone Magmatism*. Cambridge: Blackwell Science.
- Taylor, S. R., and McLennan, S. M. (1995). The Geochemical Evolution of the Continental Crust. *Rev. Geophys.* 33, 241-265. doi:10.1029/95rg00262
- Ukar, E., and Cloos, M. (2014). Low-temperature Blueschist-Facies Mafic Blocks in the Franciscan Mélange, San Simeon, California: Field Relations, Petrology, and counterclockwise P-T paths. *Geol. Soc. Am. Bull.* 126, 831-856. doi:10.1130/b30876.1
- Ulmer, P. (2001). Partial Melting in the Mantle Wedge - the Role of H₂O in the Genesis of Mantle-Derived 'Arc-Related' Magmas. *Phys. Earth Planet. Inter.* 127, 215-232. doi:10.1016/s0031-9201(01)00229-1
- Vannucchi, P., Sage, F., Phipps Morgan, J., Remitti, F., and Collot, J.-Y. (2012). Toward a Dynamic Concept of the Subduction Channel at Erosive Convergent Margins with Implications for Interplate Material Transfer. *Geochem. Geophys. Geosyst.* 13. doi:10.1029/2011gc003846
- Wakabayashi, J. (2012). Subducted Sedimentary Serpentinite Mélanges: Record of Multiple Burial-Exhumation Cycles and Subduction Erosion. *Tectonophysics* 568-569, 230-247. doi:10.1016/j.tecto.2011.11.006
- Wang, K., and Bilek, S. L. (2014). Invited Review Paper: Fault Creep Caused by Subduction of Rough Seafloor Relief. *Tectonophysics* 610, 1-24. doi:10.1016/j.tecto.2013.11.024
- Wang, Y., Foley, S. F., and Prelević, D. (2017). Potassium-rich Magmatism from a Phlogopite-free Source. *Geology* 45, 467-470. doi:10.1130/g38691.1
- Watts, A., Koppers, A., and Robinson, D. (2010). Seamount Subduction and Earthquakes. *Oceanogr.* 23, 166-173. doi:10.5670/oceanog.2010.68
- Wei, W., Kastner, M., Deyhle, A., and Spivack, A. J. (2006). "Geochemical Cycling of Fluorine, Chlorine, Bromine, and Boron and Implications for Fluid-Rock Reactions in Mariana Forearc, South Chamorro Seamount, ODP Leg 195," in *Proc. ODP, Sci. Results*. Editors M. Shinohara, M. H. Salisbury, and C. Richter (College Station, TX: Ocean Drilling Program), 195, 1-23. doi:10.2973/odp.proc.sr.195.106.2005
- Wessel, P., Smith, W. H. F., Scharroo, R., Luis, J., and Wobbe, F. (2013). Generic Mapping Tools: Improved Version Released. *Eos Trans. AGU* 94, 409-410. doi:10.1002/2013eo450001
- Wheat, C. G., Fournier, T., Paul, C., Menzies, C. D., Price, R. E., Ryan, J. G., et al. (2018). "Data Report: IODP Expedition 366 Pore Water Trace Element (V, Mo, Rb, Cs, U, Ba, and Li) Compositions," in *Proc. IODP*. Editors P. Fryer, C. G. Wheat, and T. Williams, and The Expedition 366 Scientists (College Station, TX: Ocean Drilling Program), 366. doi:10.14379/iodp.proc.366.201.2018
- White, R. W., Powell, R., Holland, T. J. B., Johnson, T. E., and Green, E. C. R. (2014b). New mineral Activity-Composition Relations for Thermodynamic Calculations in Metapelitic Systems. *J. Metamorph. Geol.* 32, 261-286. doi:10.1111/jmg.12071
- White, R. W., Powell, R., and Holland, T. J. B. (2007). Progress Relating to Calculation of Partial Melting Equilibria for Metapelites. *J. Metamorph. Geol.* 25, 511-527. doi:10.1111/j.1525-1314.2007.00711.x
- White, R. W., Powell, R., and Johnson, T. E. (2014a). The Effect of Mn on mineral Stability in Metapelites Revisited: New a-x Relations for Manganese-Bearing Minerals. *J. Metamorph. Geol.* 32, 809-828. doi:10.1111/jmg.12095
- Zack, T., Rivers, T., and Foley, S. (2001). Cs-Rb-Ba Systematics in Phengite and Amphibole: an Assessment of Fluid Mobility at 2.0 GPa in Eclogites from Tressolmen, Central Alps. *Contrib. Mineral. Petrol.* 140, 651-669. doi:10.1007/s004100000206
- Zhou, Z., and Lin, J. (2018). Elasto-plastic Deformation and Plate Weakening Due to normal Faulting in the Subducting Plate along the Mariana Trench. *Tectonophysics* 734-735, 59-68. doi:10.1016/j.tecto.2018.04.008

Conflict of Interest: The authors declare that the research was conducted in the absence of any commercial or financial relationships that could be construed as a potential conflict of interest.

Publisher's Note: All claims expressed in this article are solely those of the authors and do not necessarily represent those of their affiliated organizations, or those of the publisher, the editors and the reviewers. Any product that may be evaluated in this article, or claim that may be made by its manufacturer, is not guaranteed or endorsed by the publisher.

Copyright © 2022 Albers, Shervais, Hansen, Ichiyama and Fryer. This is an open-access article distributed under the terms of the Creative Commons Attribution License (CC BY). The use, distribution or reproduction in other forums is permitted, provided the original author(s) and the copyright owner(s) are credited and that the original publication in this journal is cited, in accordance with accepted academic practice. No use, distribution or reproduction is permitted which does not comply with these terms.